

Deep SDSS Optical Spectroscopy of Distant Halo Stars

III. Chemical analysis of extremely metal-poor stars.

E. Fernández-Alvar¹, C. Allende Prieto^{2,3}, T. C. Beers⁴, Y. S. Lee⁵, T. Masseron⁶, and D. P. Schneider⁷

¹ Instituto de Astronomía, Universidad Nacional Autónoma de México, AP 70-264, 04510 Ciudad de México, México
e-mail: emma@astro.unam.mx

² Instituto de Astrofísica de Canarias, Vía Láctea, 38205 La Laguna, Tenerife, Spain

³ Universidad de La Laguna, Departamento de Astrofísica, 38206 La Laguna, Tenerife, Spain

⁴ Department of Physics and JINA Center for the Evolution of the Elements, University of Notre Dame, Notre Dame, IN, 46556, USA

⁵ Department of Astronomy and Space Science, Chungnam National University, 99 Daehak-ro, Daejeon 34134, Republic of Korea

⁶ Institute of Astronomy, University of Cambridge, Madingley Road, CB3 0HA, Cambridge, United Kingdom

⁷ Department of Astronomy and Astrophysics, The Pennsylvania State University, University Park, PA 16802, USA

Received May 2016; accepted xxxx

ABSTRACT

Aims. We present the results of an analysis for 107 extremely metal-poor (EMP) stars with metallicities less than $[\text{Fe}/\text{H}] = -3.0$, identified from medium-resolution spectra in the Sloan Digital Sky Survey (SDSS). Our analysis provides estimates of the stellar effective temperatures and surface gravities, as well as iron, calcium, and magnesium abundances.

Methods. We follow the same methodology as in previous papers of this series, based on comparisons of the observed spectra with synthetic spectra. The abundances of Fe, Ca, and Mg are determined by fitting spectral regions dominated by lines of each element. In addition, we present a technique to determine upper limits for elements whose features are not detected in a given spectrum. We also analyse our sample with the SEGUE Stellar Parameter Pipeline, in order to obtain additional determinations of the atmospheric parameters, iron and alpha-element abundances, to compare with ours, and to infer $[\text{C}/\text{Fe}]$ ratios.

Results. We find that, in these moderate to low signal-to-noise and medium-resolution spectra in this metallicity regime, Ca is usually the only element that exhibits lines that are sufficiently strong to reliably measure its abundance. Fe and Mg exhibit weaker features that, in most cases, only provide upper limits. We measure $[\text{Ca}/\text{Fe}]$ and $[\text{Mg}/\text{Fe}]$ for EMP stars in the SDSS spectra, and conclude that most of the stars exhibit the usual level of enhancement for α -elements, $\sim +0.4$, although a number of stars for which only $[\text{Fe}/\text{H}]$ upper limits could be estimated point to higher $[\alpha/\text{Fe}]$ ratios. We also find that 26% of the stars in our sample can be classified as carbon-enhanced metal-poor (CEMP) stars, and that the frequency of CEMP stars also increases with decreasing metallicity, as has been reported for previous samples. We identify a rare, bright ($g = 11.90$) EMP star, SDSS J134144.61+474128.6, with $[\text{Fe}/\text{H}] = -3.27$, $[\text{C}/\text{Fe}] = +0.95$, and elevated magnesium ($[\text{Mg}/\text{Fe}] = +0.62$), an abundance pattern typical of CEMP-no stars.

Key words. stars: abundances, population III – Galaxy: stellar content, halo

1. Introduction

Very metal-poor (VMP; $[\text{Fe}/\text{H}] < -2.0$) and extremely metal-poor (EMP; $[\text{Fe}/\text{H}] < -3.0$) stars provide the opportunity to deepen our understanding of the early chemical evolution of the Milky Way and the Universe. In most cases, their atmospheres exhibit the chemical compositions of the gas from which they formed, enriched by the nucleosynthetic yields of the first stellar populations. In addition, recent investigations of the Milky Way's stellar halo have revealed that it is not a homogeneous entity, but rather, comprises multiple populations (Carollo et al. 2007, 2010; de Jong et al. 2010; Nissen & Schuster 2010, 2011; Beers et al. 2012; An et al. 2013, 2015; Allende Prieto et al. 2014; Chen et al. 2014; Janesh et al. 2016). Thus, VMP and EMP stars are useful probes of the assembly of the Galaxy as well.

Early survey work, e.g., the HK survey of Beers and colleagues (Beers et al. 1985, 1992) and the Hamburg/ESO survey of Christlieb and collaborators (Reimers & Wisotzki 1997; Christlieb 2003), provided the first large lists of several thousand VMP and EMP stars. More recently, advances in astronomical instrumentation has enabled multiplexed spectroscopy of even larger numbers of (generally fainter) stars, e.g., the Sloan Digital Sky Survey (SDSS; York et al. 2000), producing samples of VMP and EMP stars covering a large range of distances from the Sun.

High-resolution spectroscopic follow-up of these targets has provided abundance measurements for numerous elements, revealing the existence of chemical peculiarities that have greatly expanded our knowledge of the different nucleosynthetic pathways that contributed to the early chemical evolution of the Galaxy (e.g., Cayrel et al. 2004; Arnone et al. 2005; Aoki et

al. 2005, 2013; Cohen et al. 2004, 2007, 2008; Bonifacio et al. 2009; Lai et al. 2009; Roederer 2009, Roederer et al. 2014). Until recently, the numbers of stars with confirmed metallicities of $[\text{Fe}/\text{H}] < -3.0$ was relatively small, making it difficult to infer the global characteristics of EMP stars. Since 2005, more than 200 stars with $[\text{Fe}/\text{H}] < -3.0$ have been confirmed, based on high-resolution spectroscopic analyses (e.g., Barklem et al. 2005; Caffau et al. 2013a,b; Yong et al. 2013), including more than 50 stars with $[\text{Fe}/\text{H}] < -3.5$, and over 20 with $[\text{Fe}/\text{H}] < -4.0$ (Barklem et al. 2005; Frebel et al. 2005, 2015; Cohen et al. 2008; Caffau et al. 2011a,b, 2012; Bonifacio et al. 2012; Aoki et al. 2013; Caffau et al. 2013b; Spite et al. 2013; Yong et al. 2013; Keller et al. 2014; Allende Prieto et al. 2015; Li et al. 2015; Placco et al. 2015; Meléndez et al. 2016).

The SDSS database comprises over 900,000 stellar spectra, and is now the dominant source of confirmed EMP stars. However, the relatively low resolution ($R \sim 2000$) and limited signal-to-noise ratios ($S/N \sim 30 - 40$) of the SDSS spectra themselves make it difficult to derive elemental abundances at very low metallicities.

This paper is the third in a series devoted to analyses of Milky Way halo stars based on the low-resolution SDSS spectroscopic data. We present 107 stars with metallicities $[\text{Fe}/\text{H}] < -3.0$ for which the stellar atmospheric parameters and chemical abundances of $[\text{Fe}/\text{H}]$, $[\text{Mg}/\text{H}]$, and $[\text{Ca}/\text{H}]$ have been estimated. We also report on a method to estimate upper limits for these abundances from the SDSS spectra. This technique enables a determination of the minimal S/N required to estimate the abundance for a given element as a function of effective temperature (T_{eff}) and surface gravity ($\log g$).

This paper is outlined as follows. In Sect. 2 we briefly discuss the data used in the analysis, which is described in Sect. 3. In this section we also introduce our method to estimate upper limits. Sect. 4 reports on a comparison with estimates from other analyses, including high-resolution spectroscopy. The results are summarized in Sect. 5. Finally, we present our conclusions and a brief discussion in Sect. 6.

2. Observations

Our stellar spectra come from the SDSS. This project, started in 2000, is now on its third extension, SDSS-IV (Alam et al. 2015), and comprises a set of surveys devoted to a variety of areas, from cosmology to the evolution of galaxies and the Milky Way to the search for extrasolar planets. Its first extension, SDSS-II, included a specific stellar project, the Sloan Extension for Galactic Understanding and Exploration (SEGUE; Yanny et al. 2009), directed at investigation of the structure, formation, and chemical evolution of the Galaxy. SEGUE-2, a sub-survey of SDSS-III (Eisenstein et al. 2011), increased the number of stellar spectra, and focused on observing distant halo stars.

SEGUE, SEGUE-2, and other SDSS programs (including the main SDSS galaxy redshift survey and BOSS, the Baryon Oscillations Spectroscopic Survey, see Dawson et al. 2013) obtain spectra for colour-selected samples of F-type main-sequence turn-off stars observed for calibration purposes. Calibration stars taken during the main survey and BOSS have the advantage of being located over the entire SDSS footprint at high Galactic latitudes (rather than the limited number of directions probed by SEGUE and SEGUE-2), and include halo stars at distances of up to ~ 100 kpc.

The spectra were obtained with a pair of spectrographs on the SDSS 2.5-m telescope (Gunn et al. 2006; Smee et al. 2013)

at Apache Point Observatory, with a wavelength-dependent resolving power of $1300 < R < 3000$ over the spectral range $\sim 3800 < \lambda < 9000 \text{ \AA}$. The spectrographs were updated before the beginning of BOSS observations, in order to increase their efficiency and spectral range (to $3600 < \lambda < 10000 \text{ \AA}$). Additional details on these spectra can be found in the technical papers of the surveys (York et al. 2000; Yanny et al. 2009; Dawson et al. 2013; Alam et al. 2015), as well as in previous papers in this series (Allende Prieto et al. 2014 and Fernández-Alvar et al. 2015; hereafter Paper I and Paper II).

3. Analysis

3.1. Measurement of stellar parameters and chemical abundances

We wish to estimate stellar atmospheric parameters and individual element abundances for a sample of extremely metal-poor stars belonging to the halo system. Following the same strategy as described in Papers I and II, we made use of the FERRE code (Allende Prieto et al. 2006) to constrain the stellar atmospheric parameters – effective temperature, T_{eff} , surface gravity, $\log g$, and the global metallicity, $[\text{M}/\text{H}]$ ¹. The search is performed by comparison with a grid of synthetic spectra covering a wide range of parameter space, seeking the minimum χ^2 using quadratic Bezier interpolation between the model spectra (Auer 2003). We employ the same 3-D spectral library (T_{eff} , $\log g$, and $[\text{M}/\text{H}]$) as in Paper I, calculated from one-dimensional plane-parallel Kurucz model atmospheres (Castelli & Kurucz 2003), which consider local thermodynamical equilibrium (LTE). The grid covers the ranges $4750 < T_{\text{eff}} < 6500 \text{ K}$, $0.5 < \log g < 4.5$, and $-5.0 < [\text{M}/\text{H}] < +0.5$, in steps of 250 K, 0.5 dex, and 0.5 dex, respectively. More details of the model atmospheres, line data, and the opacities used in the generation of the spectral library can be found in Paper I.

The FERRE routine enables searches for one, several, or all of the atmospheric parameters in a library of synthetic spectra. Once the atmospheric parameters are determined, we search for a limited set of elemental abundances, holding the atmospheric parameters fixed from the analysis of the full spectrum. In our model grids we vary the abundances of all metals relative to hydrogen in solar proportions (with the exception of the α -elements, which are enhanced by +0.4 dex for metal-poor stars). Searching for $[\text{M}/\text{H}]$, but restricting the fit to regions dominated by individual lines of other elements, enables estimation of the abundance of each of those elements, corresponding to the value of $[\text{M}/\text{H}]$ that best reproduces the shapes of their associated lines. A more detailed explanation can be found in Paper II.

We first estimate the stellar parameters using the full spectral range provided by the observations. The spectral range was limited to $3850 < \lambda < 9190 \text{ \AA}$ to ensure consistency with our previous analysis in Papers I and II, which examined both the BOSS spectra and those from earlier SDSS/SEGUE observations. From this analysis we select our primary targets to have metallicities in the range $-4.0 < [\text{M}/\text{H}] < -3.0$. We reject spectra that appear to be double-lined binaries or white dwarfs. The S/N ratio (calculated as the median value per pixel in the range $4885 < \lambda < 5500 \text{ \AA}$ for each spectrum) varies between 20 <

¹ We adopt the notation $[\text{X}/\text{H}] = \log_{10} \left(\frac{N(\text{X})}{N(\text{H})} \right) - \log_{10} \left(\frac{N(\text{X})}{N(\text{H})} \right)_{\odot}$, where X is any chemical element, $N(\text{X})$ is the number density of nuclei of this element, and $N(\text{H})$ is the number density of hydrogen nuclei. $[\text{M}/\text{H}]$ is the iron abundance determined from fitting the available spectral range, which includes spectral features from other metals.

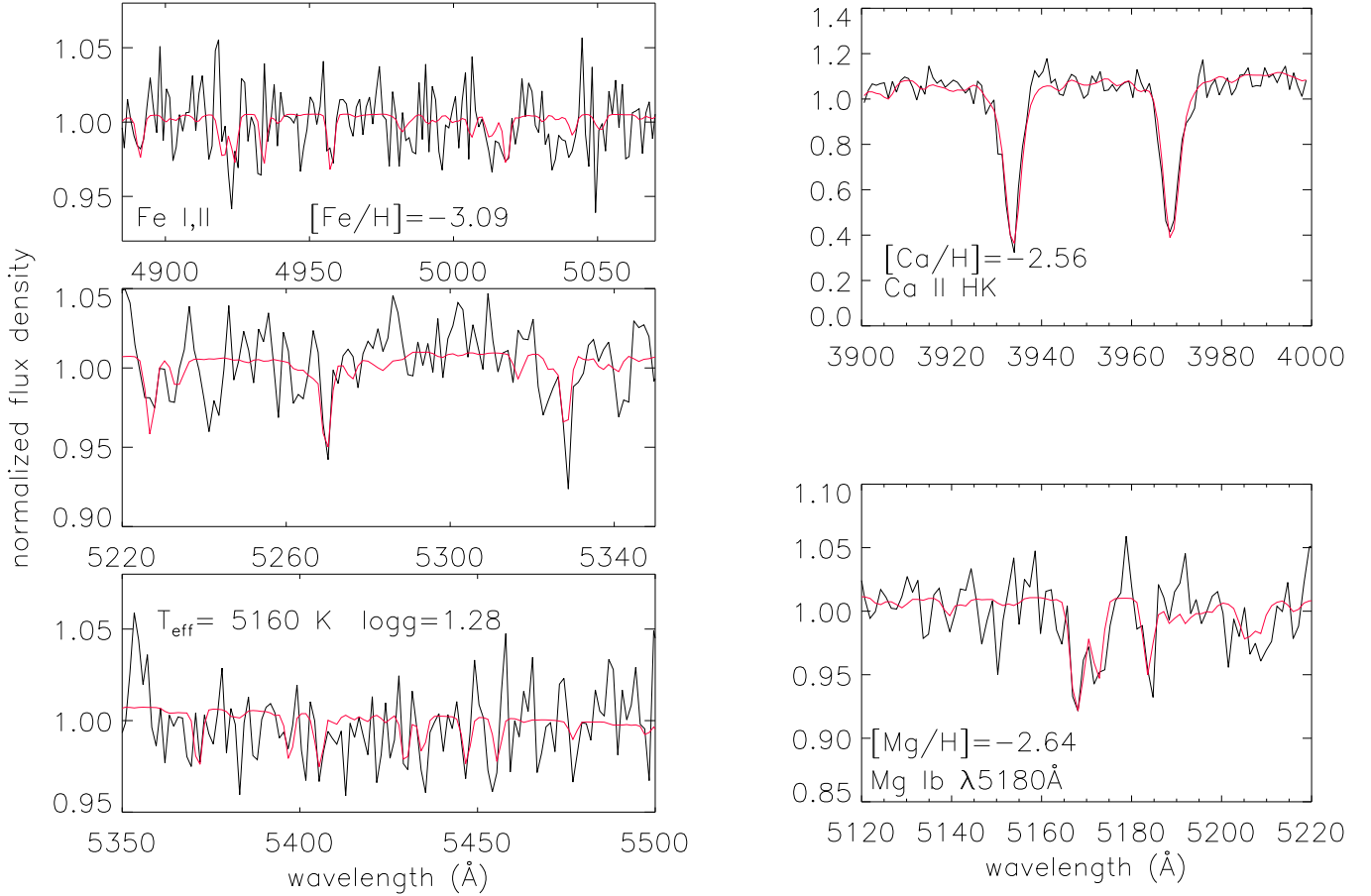


Fig. 1. Model fits for a SDSS/SEGUE star, SDSS J093339.24+310245.4, with the mean S/N of the sample, ~ 40 . The three panels in the left column correspond to the fit regions from which the $[\text{Fe}/\text{H}]$ abundance was determined. The derived iron abundance is shown in the legend of the upper panel, while the temperature and surface gravity estimates are shown in the legend of the lower panel. The panels in the right column show the CaII HK doublet and the MgIb triplet that were fit to determine Ca and Mg abundances, with the derived estimates shown in the legends.

$S/N < 90$; the derived values of T_{eff} and $\log g$ varied between $5170 < T_{\text{eff}} < 6500$ K and $0.5 < \log g < 4.5$, respectively. Holding T_{eff} and $\log g$ fixed, we repeat the search in the $[\text{M}/\text{H}]$ dimension of the grid by fitting selected regions in the spectra that contain atomic lines of Fe, Ca, or Mg.

In this analysis we fit the following spectral ranges (shown in Figure 1): $4885 < \lambda < 5070$ Å, $5220 < \lambda < 5280$ Å, $5295 < \lambda < 5500$ Å to determine Fe abundances; $5160 < \lambda < 5190$ Å (the Mg Ib triplet) for Mg abundances; and $3910 < \lambda < 3990$ Å (the Ca II H and K resonance doublet) for Ca abundances. These are the regions with the highest sensitivity in the optical spectral range for each element. The spectra were normalized by splitting them in 100 Å pieces (200 Å for the Fe I window between 4875 and 5510 Å) and dividing each piece by its mean flux value. Our synthetic spectra were treated in the same manner. From the new metallicity estimates, we obtained the abundance values of $[\text{Mg}/\text{H}]$ and $[\text{Ca}/\text{H}]$ ($[\text{Fe}/\text{H}]$ is straightforward), considering the relation with $[\text{Fe}/\text{H}]$ adopted in the construction of the spectral grid.

3.2. A method to estimate upper limits

The relatively low S/N and modest resolution of our data complicate the estimation of some elemental abundances, in particular

for Fe and Mg, whose line detections become marginal for low metallicities at the S/N of our spectra. For this reason, we developed a methodology to determine upper limits on the abundance of an element as a function of S/N, T_{eff} , $\log g$, and metallicity, $[\text{M}/\text{H}]$.

We simulated the observed spectra by smoothing our spectral library to $R = 2000$ and adding Gaussian noise. From a simulated spectrum with a particular S/N, T_{eff} , $\log g$, and $[\text{M}/\text{H}]$ (hereafter $[\text{M}/\text{H}]_0$), we evaluated the χ^2 and its error ($\sigma = \sqrt{4\chi^2}$), comparing with noise-free spectra over $-5.0 < [\text{M}/\text{H}] < -2.5$ for the same spectral windows used to determine the abundances of Fe, Mg, and Ca. We calculated the slope of the χ^2 curve in the range $-5.0 < [\text{M}/\text{H}] < [\text{M}/\text{H}]_0$. Figure 2 illustrates the methodology. Repeating this process at different S/N ratios, from 20 to 90 (in steps of 5), we defined the minimum S/N (hereafter S/N_0) at which the slope becomes significant (i.e., its error is lower than its value) for each $[\text{M}/\text{H}]_0$. This calculation was performed a hundred times to statistically refine this minimum S/N_0 value.

Evaluating simulations at T_{eff} values from 4750 to 6500 K in steps of 250 K, two $\log g$ values, 1.5 and 4.2, and metallicities from -4.8 to -2.5 in steps of 0.1 dex, we established the minimum S/N_0 vs. $[\text{Fe}/\text{H}]_0$ limit curves for each combination of stellar atmospheric parameters. The S/N range considered was 20-90 in the cases of Fe and Mg. We extended the lower limit down to $S/N = 5$ in the Ca evaluation, since the S/N over

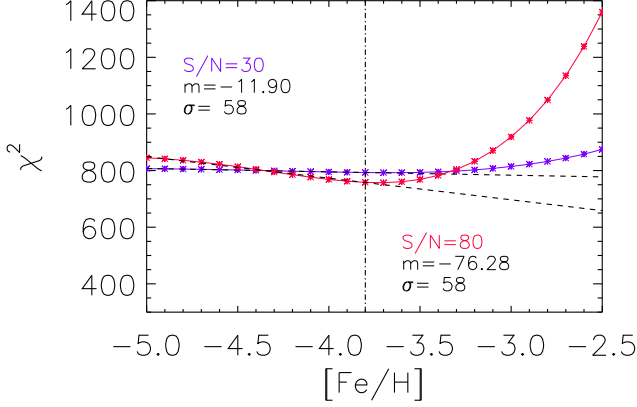


Fig. 2. The χ^2 obtained from the evaluation of a simulated spectrum at $[M/H]_0 = [Fe/H]_0 = -3.8$ (marked with a vertical dotted line) compared with synthetic spectra over a range of metallicities $[M/H]$ (from -5.0 to -2.5 with a step of 0.1 dex). The blue line shows the resulting χ^2 curve for a simulation with $S/N = 30$, and the red line applies to $S/N = 80$. The two black dotted lines indicate the linear fits up to the $[M/H]_0$ corresponding to the minimum χ^2 , from which the slope and its uncertainty are derived.

$3900 < \lambda < 4000 \text{ \AA}$ in the analysed spectra is lower than 20 in some cases. These curves were used to evaluate the reliability of our Fe, Mg, and Ca abundance determinations. Figure 3 shows the results for the case of $\log g = 1.5$ and 4.2 . We accepted a given abundance determination when it was higher than the corresponding S/N at which the modulus of the difference with the S/N of the observation is smallest. Otherwise, if the value determined by FERRE is lower than this limit, we considered the estimate as an upper limit for the abundance.

This method can be used for the analysis of low-resolution, low- S/N spectra. From Figure 3 we can infer that T_{eff} impacts determination of the abundances of the three elements considered more than $\log g$, as expected.

Iron is the element that is most difficult to measure. Although the number of available lines is larger than for the other two elements, their weakness in this metallicity regime makes them challenging to measure in the presence of noise. Our calculations indicate that a $S/N > 90$ is necessary to reliably determine $[Fe/H] \leq -4.2$ over the T_{eff} and $\log g$ ranges considered and our selected spectral range. At $S/N \sim 90$, the upper limit changes by ~ 1 dex, from -4.0 to -3.0 , between 4750 to 6500 K at $\log g = 1.5$ (becoming larger as $\log g$ increases). By contrast, the calcium abundance can be measured down to $[Ca/H] \sim -4.2$ for spectra with a median $S/N \sim 10$ for stars with $T_{\text{eff}} = 4750 \text{ K}$ and $\log g = 4.2$.

In order to provide a convenient tool to estimate the minimum S/N required to measure the abundances of these elements from the spectral windows considered in this work, we derived an analytic function that fits the curves obtained from the simulations. We found that these curves can be well-reproduced by a second-order polynomial (a convex parabola) and a straight line through the vertex of the parabola.

$$S/N = \begin{cases} a(T_{\text{eff}})[X/H]^2 + b(T_{\text{eff}})[X/H] + c(T_{\text{eff}}) & \text{if } [X/H] < \frac{-b}{2a} \\ d(T_{\text{eff}})[X/H] + e(T_{\text{eff}}) & \text{if } [X/H] > \frac{-b}{2a} \end{cases}$$

We model the dependence of the polynomial coefficients with T_{eff} as second-order polynomials. The domain of applica-

Table 1. Second-order polynomial coefficients that reproduce the parabolic and linear polynomial parameters, as a function of T_{eff} , for each of the $\log g$ values considered, 1.5 and 4.2 , for estimation of Fe.

Fe		$\log g = 1.5$	
$T_{\text{eff}} < 5500 \text{ K}$			
p_1	$-1.122267\text{e}-04$	$1.116517\text{e}+00$	$-2.725528\text{e}+03$
p_2	$-7.752576\text{e}-04$	$7.661329\text{e}+00$	$-1.862050\text{e}+04$
p_3	$-1.307124\text{e}-03$	$1.285527\text{e}+01$	$-3.112059\text{e}+04$
$T_{\text{eff}} > 5500 \text{ K}$			
p_1	$-4.702741\text{e}-05$	$5.608045\text{e}-01$	$-1.619006\text{e}+03$
p_2	$-2.673086\text{e}-04$	$3.143082\text{e}+00$	$-8.982544\text{e}+03$
p_3	$-3.688757\text{e}-04$	$4.301038\text{e}+00$	$-1.219482\text{e}+04$
l_1	$-1.493794\text{e}-02$	$6.539818\text{e}+01$	
l_2	$-3.479122\text{e}-02$	$1.706138\text{e}+02$	
Fe		$\log g = 4.2$	
$T_{\text{eff}} < 6000 \text{ K}$			
p_1	$6.350261\text{e}-05$	$-6.807567\text{e}-01$	$1.868088\text{e}+03$
p_2	$4.025916\text{e}-04$	$-4.391630\text{e}+00$	$1.219878\text{e}+04$
p_3	$6.643223\text{e}-04$	$-7.321549\text{e}+00$	$2.047375\text{e}+04$
$T_{\text{eff}} > 6000 \text{ K}$			
p_1	$4.131073\text{e}-04$	$-4.953010\text{e}+00$	$1.490776\text{e}+04$
p_2	$2.245832\text{e}-03$	$-2.701466\text{e}+01$	$8.152300\text{e}+04$
p_3	$3.071746\text{e}-03$	$-3.703024\text{e}+01$	$1.119596\text{e}+05$
l_1	$-5.311476\text{e}-03$	$1.899590\text{e}+01$	
l_2	$-7.989891\text{e}-03$	$3.985540\text{e}+01$	

bility for each second-order polynomial is defined below and above certain T_{eff} values (5500 K at $\log g = 1.5$ and 6000 K at $\log g = 4.2$).

$$a(T_{\text{eff}}) = p_{11}T_{\text{eff}}^2 + p_{12}T_{\text{eff}} + p_{13} \quad (1)$$

$$b(T_{\text{eff}}) = p_{21}T_{\text{eff}}^2 + p_{22}T_{\text{eff}} + p_{23} \quad (2)$$

$$c(T_{\text{eff}}) = p_{31}T_{\text{eff}}^2 + p_{32}T_{\text{eff}} + p_{33} \quad (3)$$

A single first-order polynomial well-fits the dependence of the other two coefficients on T_{eff} ,

$$d(T_{\text{eff}}) = l_{11}T_{\text{eff}} + l_{12} \quad (4)$$

$$e(T_{\text{eff}}) = l_{21}T_{\text{eff}} + l_{22} \quad (5)$$

Tables 1, 2, and 3 show the coefficients of these polynomials for each element for the two $\log g$ values evaluated, 1.5 and 4.2 .

4. Verification with other analyses

4.1. Comparison with the SSPP analysis

The SEGUE Stellar Parameter Pipeline (SSPP) was developed to analyse the stellar spectra gathered in the SDSS/SEGUE surveys (see Lee et al. 2008a,b; Allende Prieto et al. 2008; Smolinski et al. 2011; Lee et al. 2011 for details), and can be used to estimate T_{eff} , $\log g$, $[Fe/H]$, and $[\alpha/Fe]^2$. Recently, the SSPP has

² The $[\alpha/Fe]$ corresponds to the $[Mg/Fe]$, $[Si/Fe]$, $[Ca/Fe]$, and $[Ti/Fe]$ global measurement, from the spectral range $4500 - 5500 \text{ \AA}$ fit to the observational data with synthetic spectra.

Table 2. The same as in Table 1, but for estimation of Mg.

Mg	log $g = 1.5$		
	$T_{\text{eff}} < 5500$ K		
p_1	1.205388e-04	-1.318294e+00	3.680773e+03
p_2	9.044162e-04	-9.930854e+00	2.772508e+04
p_3	1.706439e-03	-1.876632e+01	5.232795e+04
	$T_{\text{eff}} > 5500$ K		
p_1	4.551823e-05	-5.582935e-01	1.766349e+03
p_2	3.205082e-04	-3.960549e+00	1.252583e+04
p_3	5.621326e-04	-6.969943e+00	2.201842e+04
l_1	-2.316824e-03	4.812897e+00	
l_2	-1.307164e-03	8.809123e+00	
Mg	log $g = 4.2$		
	$T_{\text{eff}} < 6000$ K		
p_1	8.279952e-05	-9.399753e-01	2.729978e+03
p_2	6.308861e-04	-7.190066e+00	2.083195e+04
p_3	1.210125e-03	-1.378693e+01	3.977522e+04
	$T_{\text{eff}} > 6000$ K		
p_1	6.482425e-06	-1.038303e-01	4.460068e+02
p_2	5.010227e-05	-8.068283e-01	3.330069e+03
p_3	1.011057e-04	-1.570228e+00	6.187633e+03
l_1	-9.710505e-04	-3.277127e+00	
l_2	4.284561e-03	-2.491109e+01	

Table 3. The same as in table 1, but for estimation of Ca.

Ca	log $g = 1.5$		
	$T_{\text{eff}} < 5500$ K		
p_1	-3.711640e-04	3.904669e+00	-1.013811e+04
p_2	-3.092381e-03	3.245765e+01	-8.415880e+04
p_3	-6.420058e-03	6.725487e+01	-1.741799e+05
	$T_{\text{eff}} > 5500$ K		
p_1	3.881031e-06	-9.518567e-02	5.899625e+02
p_2	2.968447e-05	-8.304656e-01	5.092121e+03
p_3	6.847159e-05	-1.908617e+00	1.119159e+04
l_1	2.485399e-04	-1.451917e+01	
l_2	7.746718e-03	-8.033748e+01	
Ca	log $g = 4.2$		
	$T_{\text{eff}} < 6000$ K		
p_1	5.989651e-05	-4.844238e-01	9.931608e+02
p_2	4.289678e-04	-3.375793e+00	6.682556e+03
p_3	7.663057e-04	-5.832676e+00	1.102958e+04
	$T_{\text{eff}} > 6000$ K		
p_1	2.605201e-05	-2.514639e-01	6.919529e+02
p_2	2.809412e-04	-3.033114e+00	8.964729e+03
p_3	7.024900e-04	-8.000266e+00	2.432530e+04
l_1	-1.835714e-03	-1.504880e+00	
l_2	4.354132e-03	-5.797910e+01	

been extended to be capable of estimating [C/Fe] as well (Lee et al. 2013). For the sake of comparison, we have also evaluated our sample of moderate-resolution SDSS spectra with this tool.

We compare the stellar parameters and abundance measurements obtained with the SSPP compared with our present analysis results. Our analysis returns a lower estimated T_{eff} with respect to the SSPP ($\delta = -353$ K), and a modest dispersion ($\sigma = 277$ K). This is not unexpected, since our method is purely spectroscopic, and the SSPP uses a combination of photometric and spectroscopic techniques. It has long been recognized

that spectroscopically-determined temperature estimates can be up to several hundred Kelvin cooler than photometric estimates. Regarding the log g estimate, a large systematic deviation exists for stars for which we obtain surface gravity estimates of log $g < 3$ ($\delta = -1.26$ dex, $\sigma = 1.56$ dex). This is again not surprising, since estimates of surface gravity are particularly challenging at low metallicity from low-S/N spectra. The [Fe/H] comparison exhibits a relatively small negative offset $\delta = -0.16$ dex, with a dispersion $\sigma = 0.33$ dex. Essentially all of this offset can be accounted for by the differences in the temperature estimates.

Finally, we compare the SSPP estimate of $[\alpha/\text{Fe}]$ with our [Ca/Fe] and [Mg/Fe] measurements. Both show an offset $\delta \sim -0.15$ dex and dispersion $\sigma \sim 0.26$ dex. Stars with the highest and lowest [Ca/Fe] and [Mg/Fe] estimates from our own estimates exhibit larger differences with respect to the SSPP results.

In order to clarify whether the differences in the estimated stellar parameters T_{eff} and log g severely impact the resulting abundance measurements, we repeat the [Fe/H], [Ca/Fe], and [Mg/Fe] determinations with FERRE, but after replacing the stellar parameters with those from SSPP. The resulting offset in the [Fe/H] determination compares better with the SSPP [Fe/H], although the dispersion increases slightly ($\delta = -0.09$ dex, $\sigma = 0.38$ dex). Conversely, the dispersion in the comparison of the SSPP $[\alpha/\text{Fe}]$ with the new [Ca/Fe] and [Mg/Fe] estimates increases by more than 0.2 dex, although the offset in the case of [Mg/Fe] is reduced from -0.14 dex to -0.01 dex. Thus, differences in T_{eff} and log g are not solely responsible for the derived abundance contrast with the SSPP.

4.2. Comparison with high-resolution analyses

There are several studies of EMP candidates from SDSS/SEGUE that have been followed-up and analysed with high-resolution spectra reported in the literature. Here we consider a comparison of our present results with these measurements.

SDSS J031745.82+002304.1 was analysed by Bonifacio et al. (2012) as one of their 16 EMP candidates found in the SDSS/SEGUE database. Our measurements for this star are in very good agreement with their estimates from high-resolution spectra. We obtain $T_{\text{eff}} = 5780$ K, log $g = 3.72$, [Fe/H] > -3.40 , [Ca/Fe] $\geq +0.62$ and [Mg/Fe] $\geq +0.21$, while they obtained $T_{\text{eff}} = 5786$ K, log $g = 4.02$, [Fe/H] $= -3.46$, [Ca/Fe] $= +0.75$ ($+0.60$ from Ca I lines) and [Mg/Fe] $= +0.38$.

Aoki et al. (2013) determined T_{eff} , log g , [Fe/H], [Ca/Fe], and [Mg/Fe] for 70 VMP and EMP stars selected from SDSS/SEGUE. Nine of these objects are in common with our sample: [Fe/H] measurements from both analyses are available for 7 stars, [Ca/Fe] for 5 stars, and [Mg/Fe] for 6 stars. Our T_{eff} estimates are offset by -241 K from the Aoki et al. results, with a dispersion $\sigma = 169$ K. The log g comparison exhibits a larger offset and dispersion, $\delta = -1.03$ dex and $\sigma = 1.21$ dex, similar to the comparison obtained with respect to the SSPP results. The [Fe/H] estimates compare reasonably well, with an offset of $\delta = -0.12$ dex and $\sigma = 0.21$ dex. The [Mg/Fe] results are only in fair agreement, $\delta = -0.08$ dex and $\sigma = 0.30$ dex. In contrast, our [Ca/Fe] estimates are 0.43 dex higher, with a dispersion of $\sigma = 0.39$ dex. However, the Aoki et al. determination of [Ca/H] in some of their stars came from the Ca I 4226 Å equivalent width, which is more sensitive to non-LTE effects than the Ca II HK doublet we have considered.

We identify SDSS J132250.59+012342.9 as an EMP star, as previously reported by Placco et al. (2015). For this star we obtained the following parameters: $T_{\text{eff}} = 5234$ K, log $g = 0.84$, [Fe/H] $= -3.32$, [Ca/Fe] $= +0.23$ and [Mg/Fe] $= +0.30$.

Placco et al. obtained a lower $T_{\text{eff}} = 5008 \pm 100$ K, a higher $\log g = 1.95 \pm 0.20$, and a lower $[\text{Fe}/\text{H}] = -3.64 \pm 0.05$, which are in reasonable agreement with our estimates. They also obtained $[\text{Ca}/\text{Fe}] = +0.23 \pm 0.08$ and $[\text{Mg}/\text{Fe}] = +0.25 \pm 0.05$, which are also in good agreement with our results.

Recently, Susmitha Rani et al. (2016) reported $[\text{Fe}/\text{H}] = -3.42 \pm 0.19$ for the star SDSS J134338.67+484426.6. This star is also included in our sample; we obtained estimates of $T_{\text{eff}} = 5307$ K, $\log g = 0.51$, $[\text{Fe}/\text{H}] < -3.7$, $[\text{Ca}/\text{H}] = -3.40$, and $[\text{Mg}/\text{H}] = -3.52$. Their temperature estimate is higher than ours, $T_{\text{eff}} = 5620$ K, and their $\log g = 3.44$ is considerably larger. We only determined an $[\text{Fe}/\text{H}]$ upper limit, which is lower than their $[\text{Fe}/\text{H}]$ measurement. They also determined $[\text{Ca}/\text{H}] = -3.23 \pm 0.16$, which is consistent with our estimate, and $[\text{Mg}/\text{H}] = -3.27 \pm 0.16$, slightly lower than our estimate.

In conclusion, the several comparisons we have performed reveal that our temperature estimates are generally lower than previously reported results, by about 200-250 K, due to our use of spectroscopic estimates, a significant under-estimate in our determination of $\log g$, a slight under-estimate of $[\text{Fe}/\text{H}]$ (understandable from the T_{eff} offset) and a dispersion ~ 0.3 dex in the derived $[\text{Ca}/\text{Fe}]$ and $[\text{Mg}/\text{Fe}]$.

5. Results

Our final sample of EMP stars is listed in Table 4, along with their *ugriz* magnitudes and heliocentric velocities, calculated by the SSPP (the typical accuracy for these velocities is on the order of 5 km/s). Tables 5 and 6 list our estimated stellar atmospheric parameters, T_{eff} , $\log g$, and $[\text{M}/\text{H}]$, and the derived abundances $[\text{Fe}/\text{H}]$, $[\text{Ca}/\text{H}]$, and $[\text{Mg}/\text{H}]$, as well as their uncertainties. The minimum χ^2 searches with FERRE were repeated 10 times, with added random noise. The uncertainties are estimated from the standard deviation. We only list stars for which we obtained $-4.0 < [\text{Fe}/\text{H}] < -3.0$. In cases for which our estimates were lower than the upper limit associated with the stellar parameters and S/N of the spectrum from which it was measured, a corresponding upper limit is stated. We obtained $[\text{Fe}/\text{H}]$ measurements for 44 SDSS/SEGUE spectra and 4 BOSS spectra, 48% and 24% of each sample, respectively. In the case of $[\text{Mg}/\text{H}]$, we determined reliable estimates for 86 (93%) and 13 (76%) of the stellar spectra in the SDSS/SEGUE and BOSS samples, respectively. The $[\text{Ca}/\text{H}]$ estimates were all reliable measurements. As noted above, Fe is the most difficult abundance to measure due to the weakness of its lines.

5.1. $[\text{Ca}/\text{Fe}]$ and $[\text{Mg}/\text{Fe}]$

The α -element enrichment is of particular interest in this extremely low-metallicity regime, since it can provide valuable information on the nucleosynthesis histories of the first generations of stars. Figure 4 shows our derived $[\text{Ca}/\text{Fe}]$ and $[\text{Mg}/\text{Fe}]$ (split into SDSS/SEGUE and BOSS stars in the top and bottom panels) as a function of $[\text{Fe}/\text{H}]$. We use arrows to indicate upper limits on $[\text{Fe}/\text{H}]$ (hence lower limits on $[\text{Ca}/\text{Fe}]$ and $[\text{Mg}/\text{Fe}]$). In cases for which neither Ca (or Mg) nor Fe abundances were determined, we plot their ratio with an asterisk. Overall, it appears that most of the stars present a value of $[\text{Ca}/\text{Fe}]$ consistent with the expected halo-star value of $\sim +0.4$. From inspection of this figure, it is apparent that, at the lowest metallicities, there are more stars above $[\alpha/\text{Fe}] = +0.4$ than below this value.

From the stars for which we obtained reliable determinations of the abundances, we took into account results for which

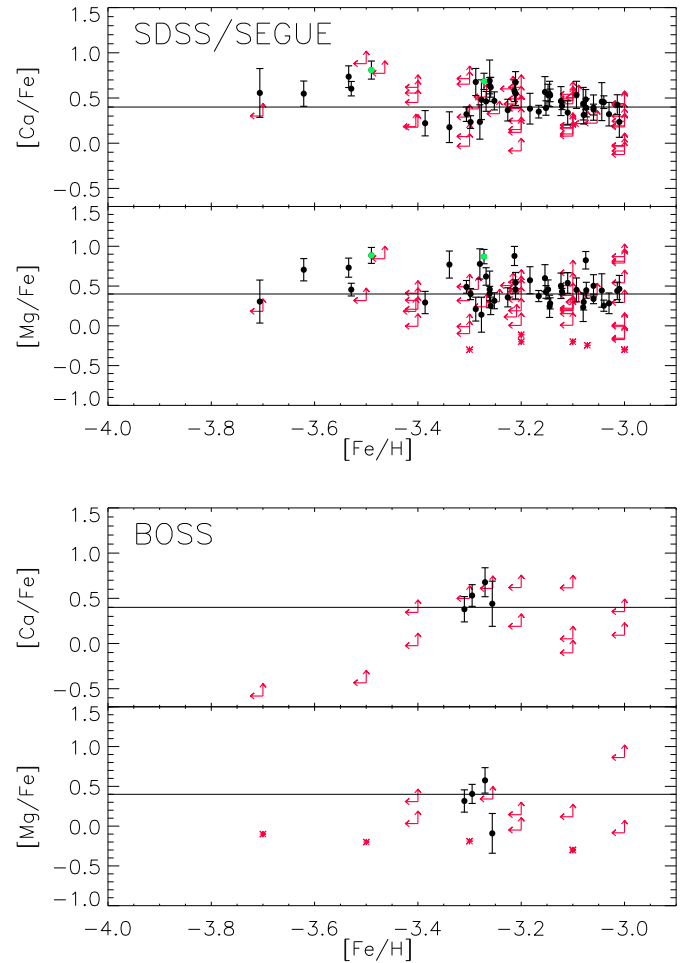


Fig. 4. $[\text{Ca}/\text{Fe}]$ and $[\text{Mg}/\text{Fe}]$ ratios, as a function of $[\text{Fe}/\text{H}]$, from the analysis of our SDSS/SEGUE and BOSS samples. The reliable estimates after applying the upper limit evaluation are indicated as black dots. Red arrows show the cases where only an upper limit for the abundances could be obtained, and the direction the ratio would be situated in this diagram. The two stars for which we obtain high $[\text{Ca}/\text{Fe}]$ and $[\text{Mg}/\text{Fe}]$ are shown as green dots.

the deviation from $[\text{Ca}/\text{Fe}] = +0.4$ was higher than three times the uncertainties of the ratios over the metallicity, or the iron abundance, in each case. We found two stars that exhibit ratios of $[\text{Ca}/\text{Fe}]$ and $[\text{Mg}/\text{Fe}]$ significantly higher than $+0.4$ among the pre-BOSS stars: SDSS J035622.42+114705.4 ($[\text{Ca}/\text{Fe}] = +0.68 \pm 0.09$; $[\text{Mg}/\text{Fe}] = +0.87 \pm 0.11$), and SDSS J031259.10-061957.1 ($[\text{Ca}/\text{Fe}] = +0.89 \pm 0.10$; $[\text{Mg}/\text{Fe}] = +0.89 \pm 0.14$). These stars are shown in Figure 4 as green dots. However, note that the SSPP estimates for these stars are $[\alpha/\text{Fe}] = +0.14$ and $+0.41$, respectively. Hence, more accurate chemical-abundance estimates are required in order to confirm their status as α -enhanced stars.

5.2. $[\text{C}/\text{Fe}]$

The SSPP provides $[\text{C}/\text{Fe}]$ measurements for 57 stars in our sample with detected carbon. After examining the resulting values, we find 28 carbon-enhanced metal-poor (CEMP) stars ($[\text{C}/\text{Fe}] > +0.7$), from which we obtain a cumulative frequency of CEMP stars below $[\text{Fe}/\text{H}] = -3.0$ of $\sim 26\%$. We also verify that the frequency of CEMP stars increases as the metallicity decreases.

Dividing our sample at the median metallicity for the stars with measured metallicity ($[\text{Fe}/\text{H}] = -3.2$), we find that $\sim 26\%$ of the stars with $-3.2 \leq [\text{Fe}/\text{H}] \leq -3.0$ are CEMP stars, while $\sim 39\%$ of the stars below $[\text{Fe}/\text{H}] = -3.2$ are CEMP stars. Note also that, below a metallicity of -3.2 , the great majority of the stars shown in Figure 5 are indeed CEMP stars, while the non-CEMP stars are the dominant fraction above this metallicity. Since over half of our stars have only upper limits for $[\text{Fe}/\text{H}]$, we have repeated the exercise with the SSPP estimates of $[\text{Fe}/\text{H}]$ for our full sample. For $[\text{Fe}/\text{H}] \leq -3.0$, we obtain a cumulative frequency of CEMP stars of $\sim 32\%$; for $[\text{Fe}/\text{H}] \leq -3.5$, the cumulative frequency increases to $\sim 42\%$. These results are consistent with the previous calculation within Poisson errors on the fractions (due to the small sample sizes involved, these are on the order of 10%).

There is no evidence of a correlation between $[\text{C}/\text{Fe}]$ and $[\text{Ca}(\text{Mg})/\text{Fe}]$, nor with the SSPP $[\alpha/\text{Fe}]$ estimates, as Figure 6 shows. Two stars exhibit high $[\text{C}/\text{Fe}]$ ($> +0.9$) as well as $[\text{Mg}/\text{Fe}]$ ($> +0.6$), but normal $[\text{Ca}/\text{Fe}]$ and $[\alpha/\text{Fe}]$.

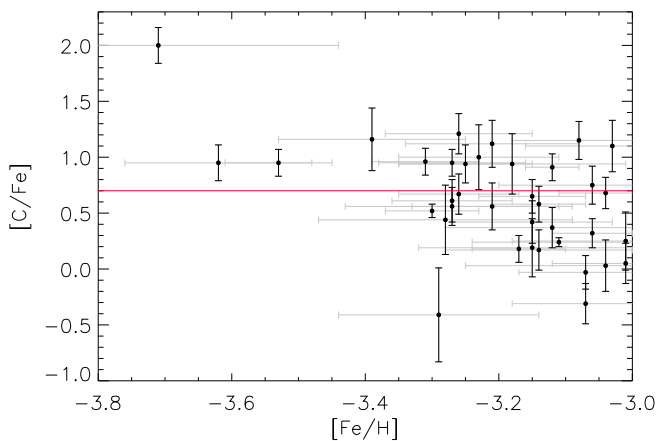


Fig. 5. $[\text{C}/\text{Fe}]$ estimates from the SSPP, as a function of our $[\text{Fe}/\text{H}]$ estimate. The red line indicates the level of $[\text{C}/\text{Fe}] > +0.7$ used to evaluate whether a star is considered carbon enhanced.

5.3. SDSS J134144.61+474128.6

We call attention to the CEMP star SDSS J134144.61+474128.6 in our sample, which is a bright ($g = 11.90$) star with $[\text{Fe}/\text{H}] = -3.27$ (the SSPP estimate of $[\text{Fe}/\text{H}] = -2.95$) and $[\text{C}/\text{Fe}] = +0.95$, identified during the course of the target search carried out for the MARVELS sub-survey (see the discussion of the MARVELS pre-survey in Rani et al. 2016). It is of interest that this star also exhibits elevated magnesium ($[\text{Mg}/\text{Fe}] = +0.62$), which is often found for CEMP-no stars (see, e.g., Norris et al. 2013). The absolute carbon abundance, $A(\text{C}) = \log \epsilon = 6.11$, places it on the “low-C” band that is associated with most CEMP-no stars (see, e.g., Bonifacio et al. 2015; Yoon et al., in prep.). We note that the other bright EMP star in our sample, discussed by Rani et al. 2016 (SDSS J134338.67+484426.6), is not carbon enhanced. Only ~ 20 EMP stars have been identified to date that are as bright as these two stars, hence we plan to obtain a higher-resolution, higher-S/N spectrum of SDSS J1341+4741 in the near future.

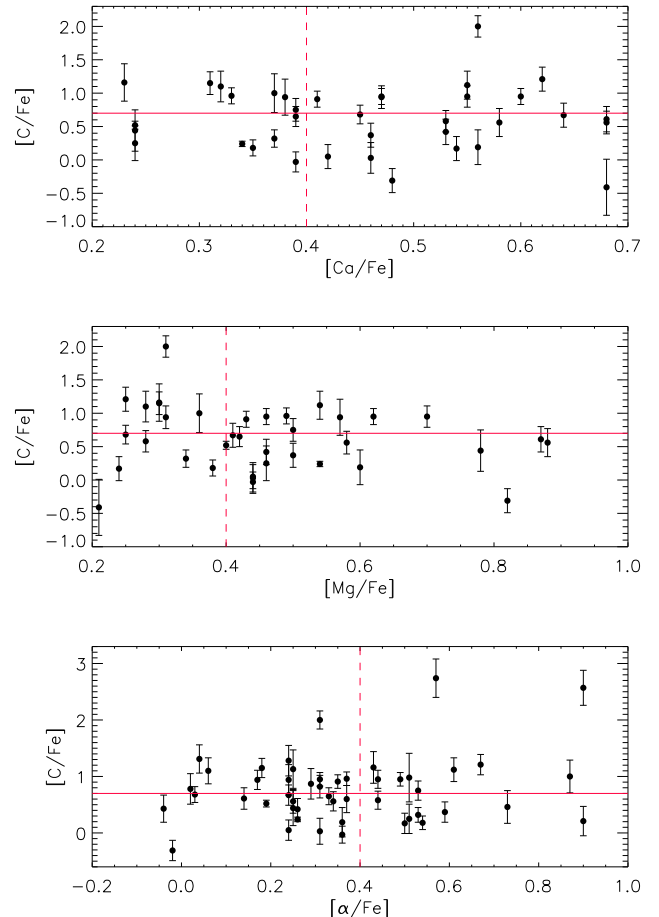


Fig. 6. $[\text{C}/\text{Fe}]$ estimates from the SSPP, as a function of our $[\text{Ca}/\text{Fe}]$ and $[\text{Mg}/\text{Fe}]$ estimates (upper two panels, respectively). The lower panel shows $[\text{C}/\text{Fe}]$ as a function of the SSPP $[\alpha/\text{Fe}]$ estimates. The red line indicates the level of $[\text{C}/\text{Fe}] > +0.7$ used to evaluate whether a star is considered carbon enhanced.

6. Conclusions

We present stellar atmospheric parameters and abundance estimates of $[\text{Fe}/\text{H}]$, $[\text{Mg}/\text{H}]$, and $[\text{Ca}/\text{H}]$ for 108 extremely metal-poor stars from SDSS/SEGUE and BOSS with iron abundances in the range $-4.0 < [\text{Fe}/\text{H}] < -3.0$. Below we summarize our main conclusions:

1. The determination of Fe and Mg abundances for EMP stars from individual lines in spectra at low spectral resolution ($R \sim 2000$) depends critically on the signal-to-noise ratio, due to the fact that these lines are weak in this metallicity range. Conversely, the Ca II HK resonance lines in the blue region of the spectrum are sufficiently strong to reliably quantify the abundance of Ca. We established a relation between S/N and $[\text{X}/\text{H}]$ in order to determine upper limits on the abundances of Fe, Ca, and Mg in cases where a reliable estimate is not possible.
2. We derive an analytical function that reproduces the detection limits for different elements as a function of S/N. These curves can be well-fit by a parabola and a linear polynomial, with coefficients that depend on T_{eff} and $\log g$. We report analytical functions that specify the minimum S/N required to reliably estimate $[\text{Fe}/\text{H}]$, $[\text{Ca}/\text{H}]$, and $[\text{Mg}/\text{H}]$ in spectra with $R \sim 2000$ and $\text{S/N} < 90$, from the spectral regions: 4885

- $< \lambda < 5070 \text{ \AA}$, $5220 < \lambda < 5280 \text{ \AA}$ and $5295 < \lambda < 5500 \text{ \AA}$ (to determine Fe); $5160 < \lambda < 5190 \text{ \AA}$ (to determine Mg abundances); and $3910 < \lambda < 3990 \text{ \AA}$ (for Ca abundances).
3. We have determined [Ca/Fe] and [Mg/Fe] abundance ratios for our program stars. The overall trend with metallicity is consistent with an α -element enhancement $[\alpha/\text{Fe}] \sim +0.4$ dex. However, a number of stars for which only Fe upper limits were estimated point to high $[\alpha/\text{Fe}]$ ratios, mainly at the lowest metallicities considered.
 4. The [C/Fe] estimates obtained with the SSPP revealed a cumulative frequency of $\sim 26\%$ CEMP stars for $[\text{Fe}/\text{H}] < -3.0$, comparable to that found by Lee et al. (2013), 28%. The frequency of CEMP stars also increases with decreasing metallicity, as reported by previous studies. We found no evidence for a [C/Fe] correlation with [Ca/Fe], [Mg/Fe], nor the SSPP $[\alpha/\text{Fe}]$ measurements.
 5. We have identified a bright ($g = 11.90$) EMP star in our sample, SDSS J134144.61+474128.6, with enhanced [C/Fe] and [Mg/Fe], as well as a low absolute carbon abundance, $A(\text{C}) = 6.11$, a pattern typically associated with CEMP-no stars. Higher resolution spectroscopic follow-up of this star is planned.

There are a number of stars with reported $[\alpha/\text{Fe}]$ significantly higher than +0.4 in the literature. For example, Aoki et al. (2007) reported on the highly α -element enhanced VMP star from the HK survey, BS 16934-002, with $[\text{Mg}/\text{Fe}] = +1.23$, but “normal” $[\text{Ca}/\text{Fe}] = +0.44$, and no carbon over-abundance. Other works reported high [C/Fe] and [Mg/Fe], but little evidence of [Ca/Fe] enhancement with respect to the typical halo values (Norris et al. 2013; Yong et al. 2013; Hansen et al. 2015). Two scenarios were proposed for this chemical pattern: i) the results of mixing and processing of material due to stellar rotation, or ii) nucleosynthesis in mixing and fallback supernova models. Elements such as Ca and Si provide the key to understanding which of these possibilities is more likely. We only found two stars for which both [C/Fe] and [Mg/Fe] are enhanced, but that exhibit normal [Ca/Fe], the expected chemical pattern for a massive spinstar (Norris et al. 2013; Maeder et al. 2015).

Puzia et al. (2006) measured $[\alpha/\text{Fe}]$ ratios significantly higher than +0.5 for globular clusters in early-type elliptical galaxies based on Lick line-index measurements, at $-1 < [\text{Z}/\text{H}]^3 < 0$. They suggest that massive stars are the potential progenitors, with $M > 20M_{\odot}$, or with $M \sim 130\text{--}190M_{\odot}$ that explode as pair-instability SNe. Both possibilities imply extremely short timescales, on the order of few Myr. Therefore, they conclude that these stars may belong to the first generation of star clusters formed in their respective galaxies. In Paper II we reported high [Ca/Fe] and [Mg/Fe] median values for stars in the outer-halo region of the Galaxy, at Galactocentric radii greater than 40 kpc. Such stars could have been formed in low-mass fragments at very early stages of the evolution of the Milky Way, and later accreted into the Galactic halo (see, e.g., Tissera et al. 2014, and references therein).

In contrast, Caffau et al. (2013a) found three stars with $[\text{Fe}/\text{H}] < -3.0$ with low $[\alpha/\text{Fe}]$ ratios. Similarly low $[\alpha/\text{Fe}]$ stars had been previously detected by Nissen and Schuster (2010). However, the latter authors found these ratios for stars with higher [Fe/H], and interpreted this population as being born after the explosion of Type Ia SNe. In this scenario, the low $[\alpha/\text{Fe}]$ ratios would then be the result of the addition of Fe from low-

to intermediate-mass stars. However, at metallicities lower than $[\text{Fe}/\text{H}] = -3.0$, few SNIa explosions are expected to have occurred. The interpretation offered by Caffau et al. (2013) is that two starbursts could have taken place in their progenitor fragment; the [low- α /Fe] ratios could then have resulted from gas enriched by SNIa explosions of stars formed in the first burst. This hypothesis was also invoked by Carigi et al. (2002) to explain low [O/Fe] in Milky Way dwarf spheroidal satellites from chemical evolution models.

It would be desirable to obtain more accurate estimates to refine our reported α -element enhancements in cases where the iron abundance could not be determined. The analysis performed in Paper II revealed high $[\alpha/\text{Fe}]$ enhancements for very metal-poor stars in the outer-halo region of our Galaxy. Accurate [Fe/H] estimates for our stars would allow us to test whether these results are confirmed by our new sample.

Acknowledgements. E.F.A. acknowledges support from DGAPA-UNAM post-doctoral fellowships. C.A.P. acknowledges support from the Spanish MINECO through grant AYA2014-56359-P. T.C.B. acknowledges partial support for this work from grants PHY 08-22648; Physics Frontier Center/Joint Institute of Nuclear Astrophysics (JINA), and PHY 14-30152; Physics Frontier Center/JINA Center for the Evolution of the Elements (JINA-CEE), awarded by the US National Science Foundation. Y.S.L. acknowledges partial support from the National Research Foundation of Korea to the Center for Galaxy Evolution Research and Basic Science Research Program through the National Research Foundation of Korea (NRF) funded by the Ministry of Science, ICT & Future Planning (NRF-2015R1C1A1A02036658). Funding for SDSS-III has been provided by the Alfred P. Sloan Foundation, the Participating Institutions, the National Science Foundation, and the U.S. Department of Energy Office of Science. The SDSS-III web site is <http://www.sdss3.org/>. SDSS-III is managed by the Astrophysical Research Consortium for the Participating Institutions of the SDSS-III Collaboration including the University of Arizona, the Brazilian Participation Group, Brookhaven National Laboratory, University of Cambridge, Carnegie Mellon University, University of Florida, the French Participation Group, the German Participation Group, Harvard University, the Instituto de Astrofísica de Canarias, the Michigan State/Notre Dame/JINA Participation Group, Johns Hopkins University, Lawrence Berkeley National Laboratory, Max Planck Institute for Astrophysics, Max Planck Institute for Extraterrestrial Physics, New Mexico State University, New York University, Ohio State University, Pennsylvania State University, University of Portsmouth, Princeton University, the Spanish Participation Group, University of Tokyo, University of Utah, Vanderbilt University, University of Virginia, University of Washington, and Yale University.

References

- Alam, S., Albareti, F. D., Allende Prieto, C., et al. 2015, *ApJS*, 219, 12
 Allende Prieto, C., Beers, T. C., Wilhelm, R., et al. 2006, *ApJ*, 636, 804
 Allende Prieto, C., Sivarani, T., Beers, T. C., et al. 2008, *AJ*, 136, 2070
 Allende Prieto, C., Fernández-Alvar, E., Schlesinger, K. J., et al. 2014, *A&A*, 568, A7
 Allende Prieto, C., Fernández-Alvar, E., Aguado, D. S., et al. 2015, *A&A*, 579, A98
 An, D., Beers, T. C., Johnson, J. A., et al. 2013, *ApJ*, 763, 65
 An, D., Beers, T. C., Santucci, R. M., et al. 2015, *ApJ*, 813, L28
 Aoki, W., Honda, S., Beers, T. C., et al. 2005, *ApJ*, 632, 611
 Aoki, W., Honda, S., Beers, T. C. et al. 2007, *ApJ*, 660, 747
 Aoki, W., Beers, T. C., Lee, Y. S., et al. 2013, *AJ*, 145, 13
 Arnone, E., Ryan, S. G., Argast, et al. 2005, *A&A*, 430, 507
 Auer, L. 2003, *Stellar Atmosphere Modeling*, 288, 3
 Barklem, P. S., Christlieb, N., Beers, T. C., et al. 2005, *A&A*, 439, 129
 Beers, T. C., Preston, G. W., & Shectman, S. A. 1985, *AJ*, 90, 2089
 Beers, T. C., Preston, G. W., & Shectman, S. A. 1992, *AJ*, 103, 1987
 Beers, T. C., Carollo, D., Ivezić, Ž., et al. 2012, *ApJ*, 746, 34
 Bonifacio, P., Spite, M., Cayrel, R., et al. 2009, *A&A*, 501, 519
 Bonifacio, P., Sbordone, L., Caffau, E., et al. 2012, *A&A*, 542, A87
 Bonifacio, P., Caffau, E., Spite, M., et al. *A&A*, 579, 28
 Caffau, E., Bonifacio, P., François, P., et al. 2011a, *Nature*, 477, 67
 Caffau, E., Bonifacio, P., François, P., et al. 2011b, *A&A*, 534, A4
 Caffau, E., Bonifacio, P., François, P., et al. 2012, *A&A*, 542, A51
 Caffau, E., Bonifacio, P., François, P., et al. 2013a, *A&A*, 560, A15
 Caffau, E., Bonifacio, P., Sbordone, L., et al. 2013b, *A&A*, 560, A71
 Carigi, L., Hernandez, X., & Gilmore, G. 2002, *MNRAS*, 334, 117
 Carollo, D., Beers, T. C., Lee, Y. S., et al. 2007, *Nature*, 450, 1020

³ These authors used $[\text{Z}/\text{H}]$ to indicate the global metallicity in a galaxy, estimated from Mg and Fe lines (see Puzia et al. 2006 and González 1993).

- Carollo, D., Beers, T. C., Chiba, M., et al. 2010, *ApJ*, 712, 692
- Cayrel, R., Depagne, E., Spite, M., et al. 2004, *A&A*, 416, 1117
- Chen, Y. Q., Zhao, G., Carrell, K., et al. 2014, *ApJ*, 795, 521
- Christlieb, N. 2003, *Reviews of Modern Physics*, 16, 191
- Cohen, J. G., Christlieb, N., McWilliam, A., et al. 2004, *ApJ*, 612, 1107
- Cohen, J. G., McWilliam, A., Christlieb, N., et al. 2007, *ApJ*, 659, L161
- Cohen, J. G., Christlieb, N., McWilliam, A., et al. 2008, *ApJ*, 672, 320
- Dawson, K. S., Schlegel, D. J., Ahn, C. P., et al. 2013, *AJ*, 145, 10
- de Jong, J. T. A., Yanny, B., Rix, H. -W., et al. 2010, *ApJ*, 714, 663
- Eisenstein, D. J., Weinberg, D. H., Agol, E., et al. 2011, *AJ*, 142, 72
- Fernández-Alvar, E., Allende Prieto, C., Schlesinger, K. J., et al. 2015, *A&A*, 577, A81
- Frebel, A., Aoki, W., Christlieb, N., et al. 2005, *Nature*, 434, 871
- Frebel, A., Chiti, A., Ji, A. P., Jacobson, H. R., & Placco, V. M. 2015, *ApJ*, 810, L27
- González, J. J. 1993, Ph.D. Thesis, University of California, Santa Cruz
- Gunn, J. E., Siegmund, W. A., Mannery, E. J., et al. 2006, *AJ*, 131, 2332
- Hansen, T., Hansen, C. J., Christlieb, N., et al. 2015, *ApJ*, 807, 173
- Janesh, W., Morrison, H.L., Ma, Z., et al. 2016, *ApJ*, 816, 80
- Keller, S. C., Bessell, M. S., Frebel, A., et al. 2014, *Nature*, 506, 463
- Lai, D. K., Rockosi, C. M., Bolte, M., et al. 2009, *ApJ*, 697, L63
- Lee, Y. S., Beers, T. C., Sivarani, T., et al. 2008a, *AJ*, 136, 2022
- Lee, Y. S., Beers, T. C., Sivarani, T., et al. 2008b, *AJ*, 136, 2050
- Lee, Y. S., Beers, T. C., Allende Prieto, C., et al. 2011, *AJ*, 141, 90
- Lee, Y. S., Beers, T. C., Masseron, T., et al. 2013, *AJ*, 146, 132
- Li, H., Aoki, W., Zhao, G., et al. 2015, *PASJ*, 67, 84
- Maeder, A., Meynet, G., & Chiappini, C. 2015, *A&A*, 576, A56
- Meléndez, J., Placco, V. M., Tucci-Maia, M., et al. 2016, *A&A*, 585, L5
- Nissen, P. E. & Schuster, W. J. 2010, *A&A*, 511, L10
- Nissen, P. E. & Schuster, W. J. 2011, *A&A*, 530, A15
- Norris, J. E., Bessell, M. S., Yong, D., et al. 2013, *ApJ*, 762, 25
- Placco, V. M., Frebel, A., Lee, Y. S., et al. 2015, *ApJ*, 809, 136
- Puzia, T. H., Kissler-Patig, M., & Goudfrooij, P. 2006, *ApJ*, 648, 383
- Reimers, D., & Wisotzki, L. 1997, *The Messenger*, 88, 14
- Roederer, I. U. 2009, *AJ*, 137, 272
- Roederer, I. U., Schatz, H., Lawler, J. E., et al. 2014, *ApJ*, 791, 32
- Smee, S. A., Gunn, J. E., Uomoto, A., et al. 2013, *AJ*, 146, 32
- Smolinski, J. P., Lee, Y. S., Beers, T. C., et al. 2011, *AJ*, 141, 89
- Spite, M., Caffau, E., Bonifacio, P., et al. 2013, *A&A*, 552, A107
- Susmitha Rani, A., Sivarani, T., Beers, T. C., et al. 2016, *MNRAS*, 458, 2648
- Tissera, P., Beers, T. C., Carollo, D., et al. 2014, *MNRAS*, 439, 2128
- Yanny, B., Rockosi, C., Newberg, H. J., et al. 2009, *AJ*, 137, 4377
- Yong, D., Norris, J. E., Bessell, M. S., et al. 2013, *ApJ*, 762, 27
- York, D. G., Adelman, J., Anderson, J. E., Jr., et al. 2000, *AJ*, 120, 1579

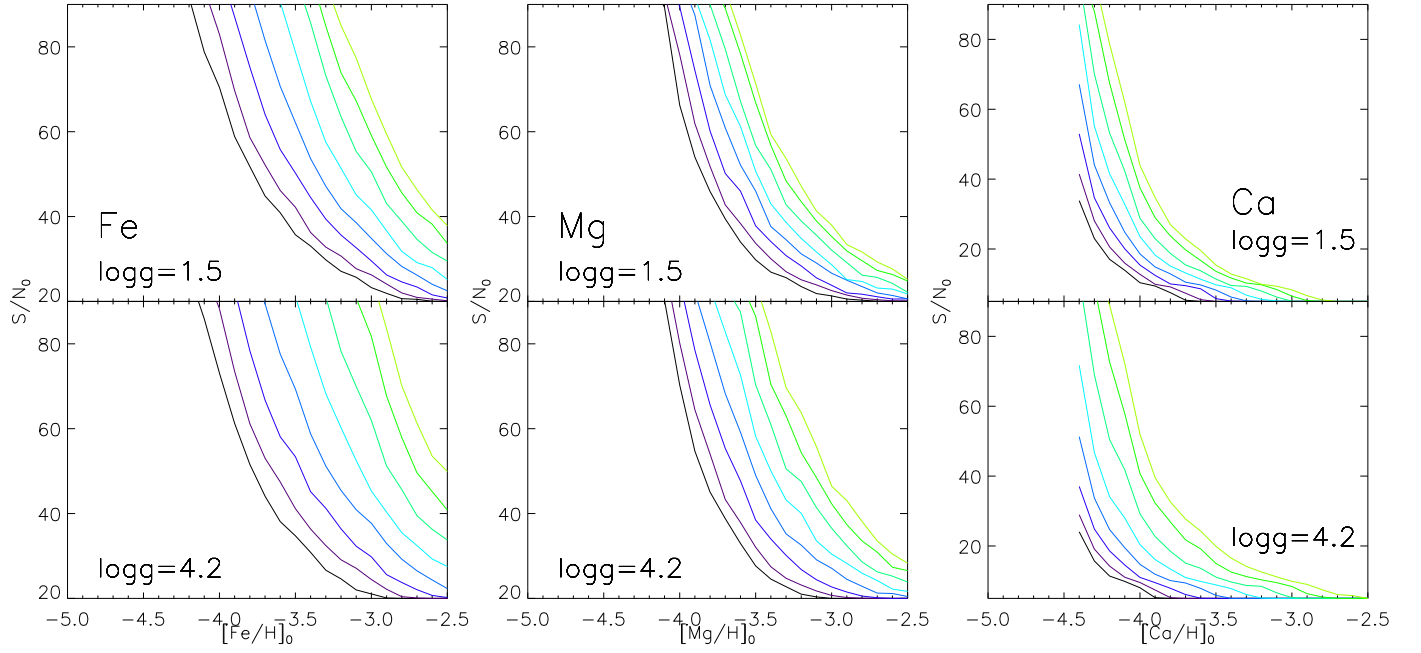


Fig. 3. Minimum signal-to-noise values, S/N_0 , required to reliably determine $[\text{Fe}/\text{H}]_0$, $[\text{Mg}/\text{H}]_0$ and $[\text{Ca}/\text{H}]_0$ minimum abundances, evaluated at $\log g = 1.5$ and $\log g = 4.5$ and $4750 < T_{\text{eff}} < 6500$ K (darker colors correspond to lower temperatures). The increase of T_{eff} complicates the $[\text{Fe}/\text{H}]$ determination, mainly in the case of Fe and Mg, and a higher S/N is necessary. The sensitivity of the Ca II HK resonance lines makes it possible to determine $[\text{Ca}/\text{H}]$ at very low abundances.

Table 4. Equatorial coordinates, SDSS magnitudes and heliocentric velocities for our SDSS/SEGUE and BOSS stellar sample.

ID	Plate-MJD-Fiber	α (J2000)	δ (J2000)	u	g	r	i	z	v_{hel} (km s ⁻¹)
SDSS J110827.88+613419.0	0775-52295-0311	167.11614	61.57199	17.78	16.96	16.67	16.57	16.54	-205.3
SDSS J115906.16+542512.6	1018-52672-0268	179.77574	54.42016	17.11	16.18	15.77	15.63	15.59	182.9
SDSS J102628.72+435742.0	1429-52990-0271	156.61971	43.96169	18.04	17.21	16.90	16.81	16.74	16.7
SDSS J235718.91-005247.7	1489-52991-0251	359.32881	-0.87994	17.20	16.06	15.43	15.15	14.99	-14.5
SDSS J191104.68+781833.6	1857-53182-0438	287.76969	78.30932	18.14	17.08	16.57	16.38	16.28	-233.6
SDSS J080428.21+515303.0	1870-53383-0002	121.11755	51.88419	17.44	16.48	16.09	15.94	15.85	-256.1
SDSS J204735.17+001137.9	1908-53239-0599	311.89656	0.19386	18.12	17.09	16.60	16.41	16.26	-206.6
SDSS J115221.93+385608.9	2027-53433-0324	178.09140	38.93580	17.48	16.64	16.26	16.10	16.09	36.5
SDSS J014036.21+234458.1	2044-53327-0515	25.15093	23.74947	16.78	15.82	15.35	15.12	15.03	-191.0
SDSS J080057.48+070550.5	2056-53463-0362	120.23952	7.09740	19.50	18.02	17.43	17.13	16.95	87.7
SDSS J161313.51+530909.6	2176-54243-0614	243.30636	53.15271	17.86	16.74	16.23	16.02	15.91	1.5
SDSS J160926.70+164743.2	2177-54557-0358	242.36125	16.79535	19.16	18.02	17.41	17.13	17.01	-27.8
SDSS J160431.54+043220.6	2178-54629-0342	241.13144	4.53908	17.74	16.72	16.23	16.03	15.94	-78.0
SDSS J180516.76+231107.7	2184-53534-0184	271.31988	23.18549	18.42	17.20	16.60	16.29	16.14	-188.4
SDSS J160142.38+053026.9	2186-54327-0277	240.42663	5.50749	19.70	18.55	18.03	17.79	17.66	-31.2
SDSS J175028.71+254434.0	2194-53904-0596	267.61965	25.74279	19.68	18.68	18.10	17.83	17.71	-407.3
SDSS J204524.03+150825.3	2250-53566-0249	311.35016	15.14041	17.84	16.76	16.22	15.94	15.83	-418.3
SDSS J220646.20-092545.7	2309-54441-0290	331.69252	-9.42937	16.68	15.36	14.74	14.44	14.28	13.2
SDSS J003910.76+082821.8	2312-53709-0575	9.79483	8.47273	19.09	18.01	17.44	17.19	17.05	-217.8
SDSS J011323.59+002631.5	2313-53726-0624	18.34832	0.44211	18.68	17.20	16.53	16.23	16.05	3.9
SDSS J225629.81+071400.5	2325-54082-0397	344.12424	7.23349	20.00	18.85	18.23	18.00	17.86	-179.3
SDSS J031119.95+060850.8	2335-53730-0465	47.83317	6.14746	18.21	17.17	16.59	16.32	16.13	40.5
SDSS J031357.33+050741.2	2340-53733-0157	48.48890	5.12813	20.11	19.05	18.39	18.11	17.92	-229.8
SDSS J023944.44+284349.7	2442-54065-0500	39.93519	28.73049	19.13	17.68	16.97	16.60	16.40	-17.0
SDSS J121042.14+402645.2	2452-54178-0506	182.67561	40.44589	17.99	16.96	16.53	16.31	16.22	-63.1
SDSS J155133.86+260423.0	2459-54544-0183	237.89113	26.07307	18.55	17.54	17.04	16.88	16.77	-99.5
SDSS J174235.90+643411.2	2561-54597-0623	265.64959	64.56979	20.61	19.20	18.58	18.30	18.12	-195.3
SDSS J215731.90+450540.7	2566-54333-0198	329.38296	45.09467	19.21	18.12	17.55	17.27	17.12	-322.8
SDSS J051803.47+180544.0	2668-54084-0368	79.51446	18.09557	18.35	17.10	16.46	16.16	15.98	-3.6
SDSS J063055.57+255243.7	2696-54167-0214	97.73157	25.87881	19.16	18.07	17.45	17.16	16.98	49.3
SDSS J173302.14+090813.3	2797-54616-0565	263.25895	9.13706	18.35	17.23	16.66	16.44	16.24	-246.0
SDSS J173532.15+444635.8	2799-54368-0502	263.88400	44.77663	17.22	15.97	15.38	15.10	15.00	-123.4
SDSS J170339.59+283650.1	2808-54524-0510	255.91500	28.61386	17.17	15.91	15.26	14.97	14.84	-174.0
SDSS J170555.89+285305.8	2808-54524-0543	256.48289	28.88498	18.56	17.38	16.81	16.54	16.41	-211.6
SDSS J170743.57+283643.1	2808-54524-0639	256.93154	28.61200	18.63	17.65	17.13	16.91	16.83	-181.4
SDSS J165835.20+272629.5	2829-54623-0281	254.64671	27.44155	19.78	18.72	18.23	18.03	17.88	63.6
SDSS J085804.66+034515.7	2888-54529-0566	134.51943	3.75437	19.44	18.32	17.84	17.61	17.49	251.1
SDSS J085934.47+040232.3	2888-54529-0615	134.89367	4.04233	17.26	16.12	15.62	15.39	15.29	155.2
SDSS J093339.24+310245.4	2889-54530-0368	143.41353	31.04594	18.91	17.60	17.07	16.81	16.67	179.5
SDSS J130615.48+390535.3	2900-54569-0312	196.56452	39.09317	18.14	17.29	16.64	16.45	16.36	-356.0
SDSS J144759.68+001308.3	2909-54653-0496	221.99868	0.21899	18.60	17.55	17.09	16.88	16.77	285.1
SDSS J085656.23+034410.3	2913-54526-0558	134.23431	3.73621	19.36	17.76	17.05	16.71	16.51	107.4
SDSS J125330.45+191331.1	2924-54582-0320	193.37690	19.22534	19.62	18.60	18.14	17.89	17.78	53.1
SDSS J143914.31+212259.4	2964-54632-0489	219.80968	21.38317	17.32	16.01	15.44	15.18	15.00	-198.8
SDSS J125050.82+102520.2	2965-54594-0461	192.71179	10.42229	18.55	17.21	16.63	16.36	16.22	73.6
SDSS J134144.61+474128.6	3003-54845-0181	205.43579	47.69100	12.66	11.90	11.34	11.19	11.25	-198.4
SDSS J134338.67+484426.6	3003-54845-0453	205.91109	48.74069	13.31	12.45	12.05	11.92	11.94	-97.4
SDSS J003529.36-111405.2	3105-54825-0010	8.87234	-11.23480	18.50	17.18	16.55	16.26	16.11	-235.4
SDSS J005420.85-003905.4	3112-54802-0282	13.58690	-0.65151	19.11	18.10	17.64	17.43	17.34	-184.3
SDSS J035622.42+114705.4	3121-54749-0496	59.09343	11.78486	19.23	18.04	17.43	17.14	16.97	-19.1
SDSS J021958.24-084955.8	3122-54821-0178	34.99267	-8.83218	17.42	16.42	15.97	15.72	15.68	-21.5
SDSS J022654.58-083951.6	3122-54821-0621	36.72738	-8.66437	18.89	17.85	17.42	17.19	17.11	-99.8
SDSS J234403.47+151744.6	3130-54740-0489	356.01446	15.29574	18.15	17.08	16.59	16.36	16.24	-293.9
SDSS J093231.65+085037.1	3151-54804-0328	143.13189	8.84365	18.99	17.70	17.05	16.81	16.63	173.0
SDSS J102328.72+352919.0	3152-54801-0068	155.86967	35.48863	18.99	17.98	17.57	17.38	17.33	-71.1
SDSS J100537.71+022734.1	3154-54821-0623	151.40716	2.45948	19.02	18.14	17.77	17.65	17.60	-0.2
SDSS J112805.85+204651.2	3170-54859-0571	172.02440	20.78090	17.18	16.07	15.56	15.38	15.20	217.1
SDSS J110445.18+670752.0	3171-54862-0412	166.18828	67.13112	17.05	16.00	15.52	15.33	15.21	-1.4
SDSS J101600.42+172901.1	3178-54848-0086	154.00179	17.48366	17.59	16.59	16.09	15.85	15.76	121.0
SDSS J120858.66+302312.9	3180-54864-0372	182.24443	30.38693	17.83	16.81	16.33	16.20	16.01	4.2

Table 4. Continued.

ID	Plate-MJD-Fiber	α (J2000)	δ (J2000)	u	g	r	i	z	v_{hel} (km s ⁻¹)
SDSS J031745.82+002304.1	3183-54833-0490	49.44092	0.38450	17.79	16.80	16.35	16.14	16.02	108.3
SDSS J025938.05+010735.3	3184-54850-0442	44.90854	1.12656	19.03	18.02	17.51	17.28	17.17	-235.2
SDSS J025956.49+005712.7	3184-54850-0451	44.98521	0.95370	18.47	16.75	15.87	15.48	15.26	36.4
SDSS J031259.10-061957.1	3186-54833-0328	48.24627	-6.33254	18.03	17.05	16.56	16.36	16.25	228.2
SDSS J033146.90+182530.7	3187-54821-0618	52.94545	18.42520	19.02	17.58	16.87	16.53	16.33	-92.0
SDSS J100401.24+420150.4	3194-54833-0090	151.00520	42.03068	18.25	17.38	17.04	16.91	16.85	42.5
SDSS J083235.90+134538.3	3195-54832-0153	128.14960	13.76065	19.31	18.06	17.40	17.12	16.94	231.2
SDSS J045637.24-044123.0	3209-54906-0287	74.15517	-4.68971	19.01	17.86	17.35	17.14	16.98	90.7
SDSS J120441.38+120111.5	3214-54866-0429	181.17244	12.01987	17.35	16.43	16.09	15.94	15.86	78.4
SDSS J082511.45+163459.9	3230-54860-0367	126.29774	16.58332	18.61	17.59	17.08	16.86	16.78	23.0
SDSS J112827.62-002232.1	3233-54891-0490	172.11511	-0.37560	17.05	15.78	15.19	14.91	14.75	175.1
SDSS J022534.63+233504.5	3241-54884-0233	36.39428	23.58458	18.96	17.97	17.51	17.33	17.21	-193.2
SDSS J115019.10+135535.4	3245-54894-0609	177.57961	13.92654	18.65	17.29	16.67	16.37	16.21	137.7
SDSS J104702.87+214308.4	3251-54882-0208	161.76198	21.71902	18.58	17.53	17.07	16.85	16.75	-39.1
SDSS J123404.57+134411.4	3254-54889-0128	188.51907	13.73652	17.80	16.87	16.46	16.29	16.19	-102.1
SDSS J104631.66+283819.7	3263-54887-0350	161.63196	28.63881	18.62	17.60	17.13	16.88	16.71	134.2
SDSS J091844.56+431219.3	3264-54889-0214	139.68568	43.20540	19.43	18.21	17.60	17.35	17.17	157.5
SDSS J082452.06+645145.6	3286-54910-0003	126.21685	64.86279	19.24	18.37	18.01	17.84	17.79	-141.5
SDSS J104617.20+172712.3	3299-54908-0450	161.57169	17.45342	17.95	16.38	15.65	15.33	15.17	170.0
SDSS J132250.59+012342.9	3307-54970-0529	200.71082	1.39528	17.47	16.32	15.82	15.60	15.49	105.5
SDSS J152853.64+065510.2	3308-54919-0513	232.22353	6.91952	19.10	17.61	16.97	16.64	16.47	-20.9
SDSS J092540.08+094104.3	3319-54915-0230	141.41699	9.68455	18.00	16.63	15.99	15.67	15.49	245.6
SDSS J111104.14+413942.6	3326-54943-0487	167.76728	41.66185	18.04	17.07	16.64	16.46	16.35	-91.4
SDSS J115525.43+474420.1	3331-54977-0355	178.85600	47.73893	18.72	17.83	17.44	17.28	17.25	67.6
SDSS J132146.89+322733.2	3377-54950-0119	200.44541	32.45924	19.46	18.49	18.01	17.87	17.75	60.0
SDSS J142928.29+295542.7	3384-54948-0172	217.36790	29.92855	17.58	16.36	15.80	15.52	15.41	-216.5
SDSS J144726.06+224552.7	3387-54951-0261	221.85861	22.76466	19.12	18.11	17.59	17.41	17.25	-250.6
SDSS J145056.30+234116.4	3387-54951-0430	222.73460	23.68791	18.36	17.23	16.71	16.49	16.35	136.1
SDSS J145124.04+093845.2	3388-54947-0187	222.85019	9.64589	18.97	17.89	17.45	17.25	17.14	115.1
SDSS J144442.53+214647.0	3407-54971-0353	221.17724	21.77972	18.73	17.70	17.22	17.00	16.86	-57.4
SDSS J165618.30+342523.0	3457-54984-0589	254.07628	34.42308	17.20	15.68	15.06	14.78	14.60	-391.6
SDSS J013643.25+010525.4	3639-55146-0544	24.18024	1.09041	18.65	17.77	17.39	17.25	17.18	-66.8
SDSS J023248.01+003735.3	3647-55827-0970	38.20007	0.62648	18.61	17.77	17.46	17.36	17.33	185.5
SDSS J024458.86+011823.8	3651-55247-0784	41.24527	1.30664	19.05	18.15	17.78	17.64	17.56	-72.3
SDSS J074449.38+471237.3	3665-55247-0074	116.20575	47.21045	17.63	16.72	16.36	16.19	16.13	231.8
SDSS J141249.08+013206.7	4030-55634-0390	213.20450	1.53520	18.94	18.08	17.69	17.53	17.45	141.9
SDSS J135331.01-032930.2	4041-55361-0401	208.37924	-3.49170	17.72	16.79	16.51	16.41	16.35	156.3
SDSS J134916.87+002622.7	4043-55630-0998	207.32032	0.43966	19.03	18.21	17.83	17.70	17.64	-36.0
SDSS J213242.72+040533.9	4084-55447-0163	323.17803	4.09275	18.70	17.88	17.56	17.45	17.38	-108.0
SDSS J084214.91+195254.9	5176-56221-0514	130.56215	19.88193	17.21	16.37	16.04	15.88	15.86	102.3
SDSS J013257.20+252558.5	5695-55978-0479	23.23836	25.43293	18.84	17.92	17.56	17.42	17.38	-232.7
SDSS J091308.43+595702.4	5712-56602-0618	138.28509	59.95079	17.23	16.31	15.92	15.76	15.74	-392.1
SDSS J092931.26+592711.7	5716-56684-0478	142.38015	59.45335	17.84	16.96	16.65	16.53	16.52	95.7
SDSS J092147.33+261936.6	5797-56273-0288	140.44724	26.32684	18.56	17.71	17.37	17.25	17.22	86.9
SDSS J004705.27+233956.0	6287-56221-0822	11.77200	23.66557	19.07	18.26	17.90	17.77	17.70	-65.4
SDSS J231319.28+211528.5	6592-56535-0046	348.33036	21.25794	20.52	19.31	18.72	18.43	18.28	-136.5
SDSS J014451.69+333127.7	6604-56337-0611	26.21538	33.52438	16.96	16.13	15.75	15.60	15.55	-143.4

Table 5. Stellar parameters T_{eff} , $\log g$ and $[M/H]$ from our analysis and the SSPP for SDSS/SEGUE and BOSS EMP stars.

Plate-MJD-Fiber	T_{eff} (K)	$\log g$	$[M/H]$	$\sigma[M/H]$	T_{eff} SSPP (K)	$\log g$ SSPP	$[\text{Fe}/H]$ SSPP
0775-52295-0311	5512	0.51	-3.17	0.91	6202	4.20	-2.52
1018-52672-0268	5488	1.62	-3.24	0.03	5852	3.34	-3.02
1429-52990-0271	5520	0.53	-3.29	0.31	6003	3.36	-2.94
1489-52991-0251	5000	4.03	-3.32	0.02	5277	3.58	-3.79
1857-53182-0438	5309	1.12	-3.17	0.04	5641	3.75	-2.84
1870-53383-0002	5529	1.17	-3.24	0.04	5989	3.55	-2.85
1908-53239-0599	5498	2.79	-3.03	0.04	5700	3.66	-3.06
2027-53433-0324	5865	4.49	-3.04	0.07	5911	4.05	-3.34
2044-53327-0515	6064	4.48	-3.42	0.05	6172	3.66	-3.30
2056-53463-0362	4781	2.23	-3.20	0.11	5349	3.56	-3.09
2176-54243-0614	4751	3.15	-3.02	0.07	5444	2.77	-2.83
2177-54557-0358	5065	4.49	-3.15	0.07	5191	3.29	-3.34
2178-54629-0342	5597	4.23	-3.00	0.11	5628	2.91	-3.11
2184-53534-0184	5116	0.63	-3.02	0.08	5440	2.82	-2.80
2186-54327-0277	5196	0.52	-3.25	0.53	5583	2.77	-3.23
2194-53904-0596	5327	4.49	-3.23	0.16	5397	3.86	-3.31
2250-53566-0249	5035	2.23	-3.59	0.05	5422	2.97	-3.38
2309-54441-0290	4902	1.49	-3.08	0.02	5175	2.43	-3.02
2312-53709-0575	5110	0.52	-3.63	0.51	5326	2.33	-3.55
2313-53726-0624	4770	0.51	-3.05	0.32	4928	1.62	-3.00
2325-54082-0397	5086	1.69	-3.08	0.06	5246	1.92	-3.16
2335-53730-0465	5255	0.55	-3.04	0.16	5929	4.03	-2.49
2340-53733-0157	5026	0.52	-3.16	0.75	5519	3.58	-2.79
2442-54065-0500	4752	2.37	-3.09	0.27	5412	2.09	-2.92
2452-54178-0506	5383	3.06	-3.07	0.04	5638	3.31	-3.09
2459-54544-0183	5653	3.89	-3.44	0.05	5697	3.56	-3.66
2561-54597-0623	4846	4.46	-3.58	0.17	4518	3.74	-3.52
2566-54333-0198	5257	0.51	-3.12	0.59	6005	4.23	-2.27
2668-54084-0368	5564	0.51	-3.00	0.27	6476	4.13	-2.31
2696-54167-0214	5399	0.53	-3.77	0.18	6088	2.87	-3.30
2797-54616-0565	5306	0.77	-3.23	0.03	5700	3.62	-2.85
2799-54368-0502	5118	1.27	-3.08	0.02	5358	3.19	-3.06
2808-54524-0510	4917	4.24	-3.40	0.04	5300	4.57	-3.44
2808-54524-0543	5136	2.42	-3.10	0.03	5438	2.59	-3.01
2808-54524-0639	5614	4.49	-3.08	0.09	5687	3.23	-2.95
2829-54623-0281	5274	0.63	-3.45	0.09	5441	2.75	-3.27
2888-54529-0566	5250	1.00	-3.07	0.04	5540	3.24	-2.87
2888-54529-0615	5194	0.95	-3.13	0.01	5520	3.18	-3.05
2889-54530-0368	5160	1.28	-3.01	0.03	5274	2.08	-2.96
2900-54569-0312	5462	4.49	-3.09	0.10	5505	4.40	-3.50
2909-54653-0496	5599	4.27	-3.25	0.10	5634	3.01	-3.26
2913-54526-0558	4873	0.82	-3.04	0.02	4812	0.83	-3.46
2924-54582-0320	5288	3.79	-3.04	0.06	5390	2.57	-2.94
2964-54632-0489	5113	1.74	-3.04	0.01	5353	2.94	-3.10
2965-54594-0461	5111	2.94	-3.08	0.02	5361	2.92	-3.28
3003-54845-0181	5254	0.51	-3.24	0.36	5808	3.38	-2.95
3003-54845-0453	5307	0.51	-3.88	0.50	6006	3.39	-3.42
3105-54825-0010	4935	0.72	-3.06	0.04	5364	2.91	-2.88
3112-54802-0282	5286	0.62	-3.18	0.07	5590	3.27	-2.83
3121-54749-0496	5305	0.85	-3.03	0.02	6002	4.08	-2.48
3122-54821-0178	5689	3.94	-3.34	0.03	5608	3.08	-3.70
3122-54821-0621	5227	0.61	-3.09	0.07	5623	3.36	-2.85
3130-54740-0489	5238	0.96	-3.38	0.01	5548	3.03	-3.32
3151-54804-0328	5004	1.20	-3.07	0.03	5360	2.58	-3.19
3152-54801-0068	5223	2.28	-3.50	0.04	5527	2.45	-3.67
3154-54821-0623	5428	0.51	-3.48	0.51	5989	3.67	-3.10
3170-54859-0571	5308	3.24	-3.05	0.02	5516	3.13	-3.22
3171-54862-0412	5283	1.21	-3.06	0.01	5569	3.26	-3.02
3178-54848-0086	5390	4.49	-3.38	0.08	5473	3.72	-3.23
3180-54864-0372	5498	4.05	-3.45	0.03	5513	3.02	-3.66

Table 5. Continued.

Plate-MJD-Fiber	T_{eff} (K)	$\log g$	[M/H]	σ [M/H]	T_{eff} SSPP (K)	$\log g$ SSPP	[Fe/H] SSPP
3183-54833-0490	5780	3.72	-3.23	0.02	5879	3.36	-3.36
3184-54850-0442	5423	4.49	-3.21	0.09	5543	3.73	-3.15
3184-54850-0451	4750	4.49	-3.19	0.21	4686	4.71	-3.44
3186-54833-0328	5130	0.51	-3.15	0.52	5682	3.83	-2.88
3187-54821-0618	4830	2.60	-3.05	0.03	5312	2.69	-2.93
3194-54833-0090	5840	3.05	-3.16	0.05	5934	3.02	-3.41
3195-54832-0153	4954	2.55	-3.19	0.06	5199	2.31	-3.10
3209-54906-0287	5060	0.81	-3.09	0.04	5469	3.05	-2.74
3214-54866-0429	5873	3.94	-3.51	0.03	5917	3.04	-3.67
3230-54860-0367	5524	3.68	-3.28	0.03	5637	3.39	-3.32
3233-54891-0490	5098	2.44	-3.32	0.02	5474	3.50	-3.32
3241-54884-0233	5492	0.54	-3.15	0.18	6152	3.83	-2.51
3245-54894-0609	4866	0.71	-3.19	0.03	5267	2.63	-3.06
3251-54882-0208	5282	3.57	-3.10	0.05	5469	3.43	-3.17
3254-54889-0128	5872	3.90	-3.53	0.05	5980	3.71	-3.46
3263-54887-0350	5207	0.72	-3.33	0.04	5539	2.62	-3.15
3264-54889-0214	5018	2.03	-3.35	0.06	5196	2.21	-3.88
3286-54910-0003	5516	0.52	-3.43	0.53	6052	3.55	-3.02
3299-54908-0450	4881	0.51	-3.04	0.12	4855	1.97	-3.23
3307-54970-0529	5234	0.84	-3.60	0.02	5536	3.25	-3.68
3308-54919-0513	4915	0.96	-3.02	0.03	5190	2.22	-3.02
3319-54915-0230	5114	1.77	-3.26	0.02	5126	2.51	-3.40
3326-54943-0487	5694	4.06	-3.02	0.03	5720	3.61	-3.20
3331-54977-0355	5760	4.49	-3.23	0.10	5879	3.82	-3.10
3377-54950-0119	5220	3.33	-3.29	0.08	5468	3.39	-3.23
3384-54948-0172	5133	1.96	-3.21	0.02	5345	2.61	-3.25
3387-54951-0261	5299	4.49	-3.37	0.14	5520	3.84	-3.35
3387-54951-0430	5231	3.12	-3.04	0.03	5457	3.31	-2.94
3388-54947-0187	5513	3.73	-3.28	0.06	5606	3.42	-3.35
3407-54971-0353	5255	2.69	-3.04	0.04	5481	2.70	-3.08
3457-54984-0589	5009	0.99	-3.11	0.01	5352	2.84	-2.99
3639-55146-0544	5488	0.52	-3.39	0.37	6015	3.29	-2.96
3647-55827-0970	5375	0.51	-3.16	0.52	6184	3.68	-2.30
3651-55247-0784	5322	0.51	-3.11	0.52	5970	3.44	-2.50
3665-55247-0074	5503	0.51	-3.37	0.27	6164	3.78	-2.70
4030-55634-0390	5572	1.02	-3.69	0.06	5993	3.09	-3.42
4041-55361-0401	5595	0.52	-3.89	0.17	6297	3.21	-3.42
4043-55630-0998	4750	3.23	-3.09	0.27	5999	3.37	-3.60
4084-55447-0163	5268	0.51	-3.53	0.70	6258	3.52	-2.60
5176-56221-0514	5426	0.51	-3.33	0.39	6112	3.86	-2.86
5695-55978-0479	5362	0.50	-3.36	1.27	6293	4.27	-2.32
5712-56602-0618	5292	0.50	-3.05	0.19	6067	4.02	-2.52
5716-56684-0478	5419	0.54	-3.40	0.16	6216	3.83	-2.56
5797-56273-0288	5419	0.51	-3.53	0.35	6116	3.59	-3.13
6287-56221-0822	5287	0.51	-3.37	0.75	5963	3.27	-3.06
6592-56535-0046	5252	0.50	-3.11	0.88	6122	3.31	-2.51
6604-56337-0611	5375	0.50	-3.20	0.46	6003	3.77	-2.76

Table 6. Chemical abundances for the SDSS/SEGUE and BOSS EMP stars.

Plate-MJD-Fiber	[Fe/H]	σ [Fe/H]	[Ca/H]	σ [Ca/H]	[Mg/H]	σ [Mg/H]	[α /Fe] SSPP	[C/Fe] SSPP
0775-52295-0311	< -3.00	-	-2.72	0.05	-2.42	0.26	0.31	-
1018-52672-0268	-3.28	0.22	-2.80	0.02	-3.14	0.24	-0.30	-
1429-52990-0271	< -3.00	-	-2.82	0.04	-3.17	0.28	-	-
1489-52991-0251	-3.62	0.14	-3.07	0.02	-2.92	0.11	0.44	0.95
1857-53182-0438	< -3.20	-	-2.71	0.05	-2.65	0.37	0.30	-
1870-53383-0002	< -3.05	-	-2.83	0.04	-2.67	0.27	0.29	-
1908-53239-0599	< -3.10	-	-2.56	0.03	-2.89	0.30	0.73	0.46
2027-53433-0324	< -3.10	-	-2.63	0.03	-2.43	0.11	0.24	-
2044-53327-0515	< -3.00	-	-3.03	0.03	-3.01	0.15	-	2.19
2056-53463-0362	< -3.20	-	-2.81	0.07	-2.77	0.30	0.51	0.98
2176-54243-0614	-3.71	0.27	-3.15	0.02	-3.40	0.10	0.31	2.00
2177-54557-0358	-3.17	0.07	-2.82	0.03	-2.79	0.07	0.54	0.18
2178-54629-0342	< -3.00	-	-2.58	0.02	-3.16	0.50	0.51	-
2184-53534-0184	-3.04	0.21	-2.58	0.04	-2.60	0.24	0.31	0.03
2186-54327-0277	< -3.07	-	-2.85	0.06	< -3.32	-	-	-
2194-53904-0596	< -3.00	-	-3.09	0.07	-2.21	0.08	0.50	-
2250-53566-0249	< -3.40	-	-3.22	0.03	-3.22	0.15	-0.04	0.43
2309-54441-0290	-3.06	0.14	-2.67	0.01	-2.56	0.10	0.53	0.75
2312-53709-0575	< -3.20	-	-3.08	0.06	< -3.40	-	-	-
2313-53726-0624	-3.21	0.12	-2.54	0.04	-2.75	0.32	0.42	-
2325-54082-0397	< -3.00	-	-2.70	0.08	< -3.30	-	-	0.25
2335-53730-0465	-3.15	0.17	-2.59	0.02	-2.55	0.20	0.36	0.19
2340-53733-0157	< -3.00	-	-2.56	0.09	-2.46	0.52	0.38	-
2442-54065-0500	< -3.24	-	-2.92	0.05	-2.94	0.25	0.24	1.28
2452-54178-0506	< -3.10	-	-2.66	0.02	-2.88	0.19	0.29	0.87
2459-54544-0183	< -3.10	-	-3.00	0.04	-2.72	0.15	0.11	-
2561-54597-0623	< -3.20	-	-3.28	0.08	-3.19	0.14	-	-
2566-54333-0198	< -3.22	-	-2.61	0.06	-2.71	0.24	0.25	1.13
2668-54084-0368	< -3.00	-	-2.56	0.03	-2.19	0.33	0.55	-
2696-54167-0214	< -3.30	-	-3.33	0.06	-3.31	0.23	-	-
2797-54616-0565	-3.18	0.17	-2.80	0.02	-2.61	0.14	0.24	0.94
2799-54368-0502	-3.29	0.15	-2.61	0.01	-3.08	0.14	-	-0.41
2808-54524-0510	-3.30	0.07	-3.06	0.01	-2.90	0.04	0.19	0.52
2808-54524-0543	< -3.46	-	-2.69	0.03	-2.62	0.14	0.04	1.31
2808-54524-0639	< -3.20	-	-2.58	0.04	-3.01	0.13	0.90	-
2829-54623-0281	< -3.10	-	-3.02	0.05	-2.95	0.35	-	-
2888-54529-0566	< -3.30	-	-2.59	0.05	-2.98	0.26	-	0.28
2888-54529-0615	-3.06	0.06	-2.69	0.01	-2.72	0.11	0.53	0.32
2889-54530-0368	-3.09	0.15	-2.56	0.03	-2.64	0.23	0.40	-0.41
2900-54569-0312	< -3.10	-	-2.61	0.04	-2.59	0.11	0.90	0.21
2909-54653-0496	< -3.20	-	-2.82	0.03	-2.73	0.13	0.30	-
2913-54526-0558	-3.04	0.07	-2.59	0.01	-2.79	0.09	0.03	0.68
2924-54582-0320	< -3.10	-	-2.93	0.07	< -3.30	-	-	1.21
2964-54632-0489	-3.14	0.14	-2.60	0.01	-2.90	0.18	0.50	0.17
2965-54594-0461	-3.12	0.04	-2.71	0.02	-2.69	0.09	0.35	0.91
3003-54845-0181	-3.27	0.11	-2.80	0.01	-2.65	0.10	0.49	0.95
3003-54845-0453	< -3.70	-	-3.40	0.02	-3.52	0.17	0.06	-
3105-54825-0010	-3.21	0.12	-2.63	0.03	-2.33	0.17	0.25	0.56
3112-54802-0282	-3.01	0.17	-2.77	0.04	-2.55	0.16	0.51	0.25
3121-54749-0496	-3.27	0.09	-2.59	0.01	-2.40	0.11	0.14	0.61
3122-54821-0178	< -3.28	-	-2.90	0.02	-2.83	0.13	0.49	-
3122-54821-0621	-3.12	0.16	-2.66	0.02	-2.62	0.15	0.59	0.37
3130-54740-0489	-3.31	0.08	-2.98	0.01	-2.82	0.11	0.37	0.96
3151-54804-0328	-3.15	0.12	-2.62	0.03	-2.69	0.17	0.26	0.42
3152-54801-0068	-3.34	0.17	-3.16	0.04	-2.57	0.17	0.30	-
3154-54821-0623	< -3.20	-	-2.95	0.05	-2.87	0.21	0.31	-
3170-54859-0571	-3.21	0.13	-2.66	0.02	-2.67	0.13	0.61	1.12
3171-54862-0412	-3.26	0.09	-2.62	0.01	-2.85	0.17	0.24	0.67
3178-54848-0086	< -3.40	-	-2.95	0.03	-3.08	0.09	0.37	0.60
3180-54864-0372	< -3.30	-	-3.23	0.02	< -3.60	-	0.90	2.57
3183-54833-0490	< -3.40	-	-2.78	0.02	-3.19	0.13	0.69	-

Table 6. Continued.

Plate-MJD-Fiber	[Fe/H]	σ [Fe/H]	[Ca/H]	σ [Ca/H]	[Mg/H]	σ [Mg/H]	$[\alpha/\text{Fe}]$ SSPP	[C/Fe] SSPP
3184-54850-0442	< -3.27	-	-2.76	0.04	-3.03	0.11	0.40	-
3184-54850-0451	-3.11	0.13	-2.77	0.02	-2.57	0.03	0.26	0.24
3186-54833-0328	< -3.30	-	-2.65	0.04	-2.81	0.25	0.49	-
3187-54821-0618	-3.08	0.10	-2.77	0.02	-2.78	0.09	0.18	1.15
3194-54833-0090	< -3.00	-	-2.81	0.04	-2.71	0.23	0.57	2.74
3195-54832-0153	< -3.50	-	-2.62	0.04	-3.18	0.23	-	1.23
3209-54906-0287	-3.26	0.23	-2.57	0.04	-2.80	0.24	0.27	-
3214-54866-0429	< -3.30	-	-3.01	0.02	-3.40	0.29	-	-
3230-54860-0367	< -3.40	-	-2.84	0.02	-2.99	0.12	0.02	0.78
3233-54891-0490	-3.53	0.08	-2.93	0.01	-3.07	0.10	0.31	0.95
3241-54884-0233	-3.08	0.18	-2.64	0.03	-2.85	0.15	0.49	-
3245-54894-0609	-3.15	0.08	-2.76	0.02	-2.73	0.13	0.33	0.65
3251-54882-0208	< -3.21	-	-2.77	0.03	-3.10	0.19	0.31	0.82
3254-54889-0128	< -3.00	-	-3.03	0.05	-2.99	0.20	0.90	-
3263-54887-0350	-3.23	0.12	-2.86	0.03	-2.87	0.23	0.87	1.00
3264-54889-0214	-3.28	0.19	-3.04	0.06	-2.50	0.22	0.25	0.44
3286-54910-0003	< -3.00	-	-3.12	0.12	-2.13	0.28	0.53	-
3299-54908-0450	-3.07	0.11	-2.59	0.02	-2.25	0.17	-0.02	-0.31
3307-54970-0529	-3.39	0.14	-3.16	0.01	-3.09	0.12	0.43	1.16
3308-54919-0513	-3.01	0.11	-2.59	0.02	-2.57	0.18	0.24	0.05
3319-54915-0230	-3.53	0.12	-2.80	0.03	-2.80	0.16	0.41	-
3326-54943-0487	< -3.09	-	-2.58	0.02	-2.79	0.17	0.04	-
3331-54977-0355	< -3.00	-	-2.76	0.04	< -3.30	-	0.22	-
3377-54950-0119	< -3.10	-	-2.90	0.08	-3.09	0.22	-	-
3384-54948-0172	-3.25	0.10	-2.78	0.02	-2.94	0.17	0.17	0.94
3387-54951-0261	< -3.20	-	-3.05	0.09	< -3.31	-	-	1.39
3387-54951-0430	-3.14	0.07	-2.61	0.02	-2.86	0.14	0.44	0.58
3388-54947-0187	< -3.10	-	-2.93	0.06	-2.91	0.19	-	-
3407-54971-0353	-3.03	0.13	-2.71	0.04	-2.75	0.20	0.06	1.10
3457-54984-0589	-3.07	0.10	-2.68	0.01	-2.63	0.09	0.36	-0.03
3639-55146-0544	< -3.10	-	-2.86	0.04	-3.16	0.26	0.59	-
3647-55827-0970	< -3.20	-	-2.58	0.05	-3.06	0.31	-0.19	-
3651-55247-0784	< -3.25	-	-2.65	0.04	-2.91	0.22	0.00	-
3665-55247-0074	-3.31	0.14	-2.93	0.01	-2.99	0.14	0.02	-
4030-55634-0390	< -3.10	-	-3.20	0.05	< -3.40	-	-0.50	-
4041-55361-0401	< -3.40	-	-3.42	0.04	-3.37	0.23	0.02	-
4043-55630-0998	< -3.50	-	-3.93	0.07	< -3.70	-	-	3.41
4084-55447-0163	< -3.10	-	-3.05	0.07	< -3.40	-	-	-
5176-56221-0514	-3.26	0.25	-2.82	0.01	-3.35	0.16	-0.35	-
5695-55978-0479	< -3.10	-	-2.48	0.16	-2.98	0.29	-	-
5712-56602-0618	-3.27	0.16	-2.59	0.03	-2.69	0.17	0.34	0.56
5716-56684-0478	< -3.30	-	-2.80	0.05	< -3.89	-	-	-
5797-56273-0288	< -3.20	-	-3.01	0.04	-3.25	0.29	-	-
6287-56221-0822	< -3.00	-	-2.91	0.07	-3.08	0.36	-	-
6592-56535-0046	< -3.00	-	-2.65	0.04	-2.14	0.40	-0.20	-
6604-56337-0611	-3.29	0.12	-2.76	0.01	-2.89	0.15	0.22	-